REPORT DOCUMENTATION PAGE

Form Approved OMB No. 0704-0188

1. REPORT DATE *(DD-MM-YYYY)*	2. REPORT TYPE	3. DATES COVERED *(From – To)*
29-09-2003	Final Report	7 February 2003 - 13-Feb-04

4. TITLE AND SUBTITLE

Rigorous Mathematical Modeling Of The Adsorption System With Electrothermal Regeneration Of The Used Adsorbent.

5a. CONTRACT NUMBER
FA8655-03-1-3010

5b. GRANT NUMBER

5c. PROGRAM ELEMENT NUMBER

6. AUTHOR(S)

Dr. Menka T Petkovska

5d. PROJECT NUMBER

5d. TASK NUMBER

5e. WORK UNIT NUMBER

7. PERFORMING ORGANIZATION NAME(S) AND ADDRESS(ES)

University of Belgrade
Faculty of NanoTechnology and Metallurgy
Belgrade 11000
Yugoslavia

8. PERFORMING ORGANIZATION REPORT NUMBER

N/A

9. SPONSORING/MONITORING AGENCY NAME(S) AND ADDRESS(ES)

EOARD
PSC 802 BOX 14
FPO 09499-0014

10. SPONSOR/MONITOR'S ACRONYM(S)

11. SPONSOR/MONITOR'S REPORT NUMBER(S)
SPC 03-3010

12. DISTRIBUTION/AVAILABILITY STATEMENT

Approved for public release; distribution is unlimited.

13. SUPPLEMENTARY NOTES

14. ABSTRACT

This report results from a contract tasking University of Belgrade as follows: The contractor shall model a known and existing single adsorber of the hollow cylinder, several layers of activated carbon cloth, radial gas flow type. Modelling will incorporate:
1. Modeling of adsorption: Models of different complexity (local equilibrium, film mass transfer with or without dispersion, pore-surface diffusion, micropore diffusion and their combinations) of the hollow-cylinder adsorber with radial gas flow will be established.
2. Modelling of heating of the bed by electric current: Model the thermal behavior of the adsorbent bed. This model will include the modelling of the electrical field within the adsorber bed as well as the dominant heat transfer mechanisms. As a result, the temperature field within the bed can be predicted.
3. Modelling of electro-thermal desorption: Integrate the thermal model and the model or models for mass transfer, chosen as the most appropriate in the first phase (modeling of adsorption). This integration is not mechanical, as there is essential coupling between the heat generation and heat transfer on one, and mass transfer on the other hand. As a result, it will be necessary to estimate additional or correct the models parameters estimated in the previous stages.

15. SUBJECT TERMS
EOARD, Thermochemical Reactors, Mathematical Modeling, adsorption

16. SECURITY CLASSIFICATION OF:			17. LIMITATION OF ABSTRACT	18, NUMBER OF PAGES	19a. NAME OF RESPONSIBLE PERSON
a. REPORT	b. ABSTRACT	c. THIS PAGE			CARL A. KUTSCHE, Lt Col, USAF
UNCLAS	UNCLAS	UNCLAS	UL		19b. TELEPHONE NUMBER *(Include area code)* +44 (0)20 7514 4505

Grant No. FA8655-03-1-3010

RIGOROUS MATHEMATICAL MODELING OF AN ADSORPTION SYSTEM WITH ELECTROTHERMAL REGENERATION OF THE USED ADSORBENT

Principal investigator:
Dr. Menka Petkovska
Department of Chemical Engineering
University of Belgrade, Serbia and Montenegro

Final Performance Report for Year 1

Modeling of a single annular, radial-flow, cartridge-type adsorption bed

PROJECT OVERVIEW

OBJECTIVES

The general objective of the project is fundamental mathematical modelling of a complex TSA system with electrothermal desorption step, and with integrated condenser of the desorbed compound, which would enable better fundamental insight in to the process and its optimization. The objective of this stage of the project is modeling of the central unit of the TSA system: the adsorption bed. The adsorbers in the TSA system under consideration consist of cartridge-type, radial flow fixed beds, made of spirally coiled activated carbon fiber clot (ACFC). Accordingly, the subject of the mathematical modeling in this project is a single annular, radial-flow, cartridge-type ACFC adsorption bed. Models of different complexity are to be postulated and used for simulation of adsorption, electroresistive heating, electrothermal desorption and consecutive adsorption-desorption in the described adsorber.

STATUS OF EFFORT

Two mathematical model of the system under consideration have been postulated: the first assuming uniform adsorbent density throughout the adsorbent bed, and the second taking into account the structure of the bed made of layers of ACFC. Both models were obtained as complex sets of coupled nonlinear PDEs, ODEs and algebraic equations, defining the equilibrium and transport parameters of the system. Numerical procedures for solving the model equations have been established and used for simulation of adsorption, electroresistive heating, electrothermal desorption and consecutive adsorption-desorption. Nevertheless, comparison with experiments couldn't be performed owing to the lack of detailed experimental data corresponding to a single cartridge adsorber. Also, lack of reliable relations for calculation of transport parameters for an adsorbent bed with fibrous structure was observed.

ACCOMPLISHMENTS /NEW FINDINGS

Mathematical models for an annular, radial-flow adsorption bed have been developed and the procedures for their numerical solutions established. These models can be used, not only for the TSA system with electrothermal desorption step, but, after minor adjustments, for other cases, with external or internal heating of the adsorption bed, as well. The models developed in this project can be used as the basic block for modeling of the entire TSA system.

PERSONNEL SUPPORTED

Danijela Antov, MS student

Dr. Menka Petkovska, Assoc. Professor

PUBLICATIONS

No publications yet.

Two journal papers in preparation:

- A review paper on electrothermal desorption
- A scientific paper based on the results presented in this report

One paper accepted for presentation at the Fundamentals of Adsorption – FOA8 Conference in Arizona, 23-27 May 2004:

- "Electrothermal desorption in an annular - radial flow – ACFC adsorber – Mathematical modeling", by M. Petkovska, D. Antov and P. Sullivan

NEW DISCOVERYS, INVENTIONS AND PATENTS:

None

DETAILED REPORT

1. Introduction

The idea about regeneration of used adsorbent beds by direct heating by passing electric current through them (owing to Joule effect), was first published in the 1970s [1]. Desorption process based on this principle was later named electrothermal desorption [2]. It was recognized as a perspective way to perform the desorption steps of TSA cycles [2]. At the same time, fibrous activated carbon was recognized as a very convenient adsorbent form for its realization [2]. In the last couple of years application of electrothermal desorption has reached the industrial scale [11, 12].

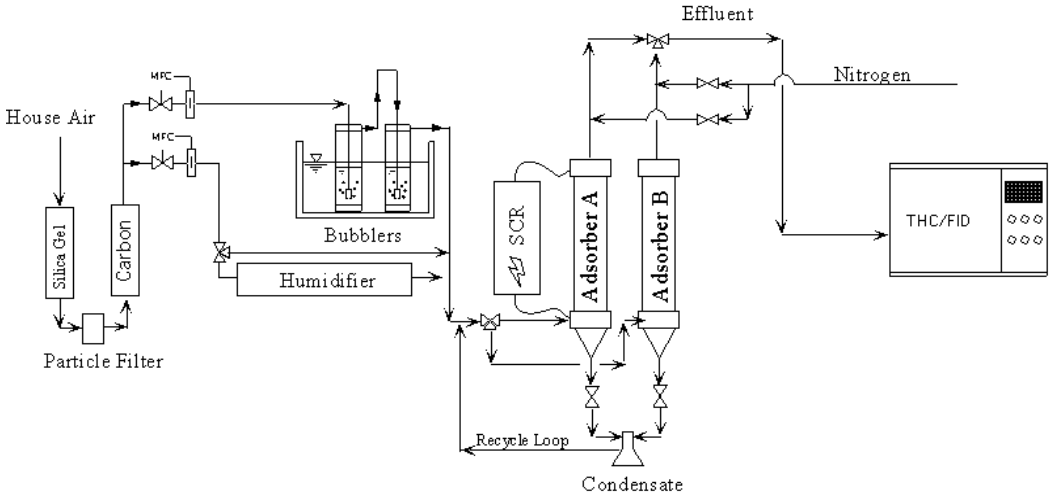

Figure 1. Overall schematic of the ACFC adsorption – rapid electrothermal desorption system (from Ref. [3])

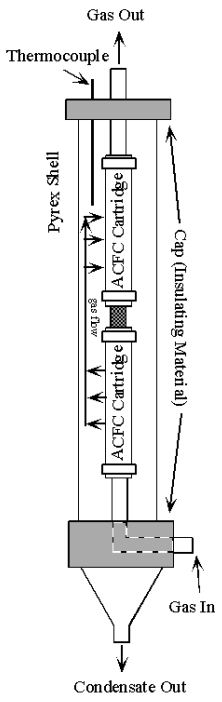

Figure 2. Structure of the adsorbers (from Ref. [3])

This project is devoted to modeling of a novel TSA system with electrothermal desorption step, described in Ref. [3], and shown in Figure 1. Each adsorber of this system consists of two annular cartridge-type fixed beds, made of activated carbon fiber cloth (ACFC) (Figure 2).

There are several reasons for developing fundamental mathematical models of the investigated process. This modeling should enable:

- Better phenomenological understanding of the process and recognizing of the most important mechanisms and phenomena;
- Better insight into the process which can help to detect it's drawbacks and to propose the necessary improvements, regarding the necessity for new measurements, potential change of the operational conditions or even potential change of the design;
- The possibility for prediction of the system behavior at different operational conditions, different scale, or with a changed design, which could substantially lower the need for experimental trials;

- Optimization of the system based on the computational analysis.

Before making an attempt to derive a complete mathematical model of this complex system, mathematical modeling of a single adsorption bed, would be very useful. This report presents the results of such modeling.

2. Description of the system - annular, radial-flow, cartridge-type adsorber

The investigation during the first year of the project ″Rigorous mathematical modeling of an adsorption system with electrothermal desorption of the used adsorbent″, was focused on mathematical modeling of a single-cartridge adsorber, for three processes that could be performed in it: adsorption, electroresistive heating and electrothermal desorption of a previously adsorbed sorbate.

The annular, radial-flow, cartridge-type fixed-bed is schematically shown in Figure 3. It is formed as a cylindrical roll of activated carbon fiber cloth (ACFC) spirally coiled around a porous central pipe, used for introducing the gas stream (the stream that has to be purified, during adsorption, or an inert gas stream, during desorption). The gas flows in the radial direction through the adsorber, leaving the adsorber through an annular space around the adsoption bed. During the desorption step, electric current is passed through the activated carbon cloth in the axial direction, causing heat generation inside the carbon fibers (Joule heat). As a result, the temperature of the carbon material increases, causing desorption.

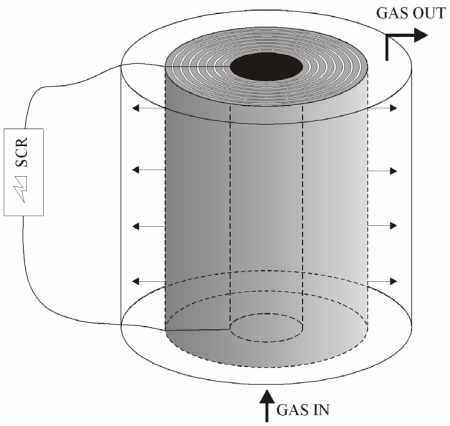

Figure 3. A schematic representation of the annular - radial flow - ACFC adsorbent bed

The adsorption process with the reversed gas flow (inlet through the outer annular pipe and outlet through the central pipe), which is also feasible in this geometry, is also considered.

Two different models of the adsorber will be present. In the first one, the adsorbent bed is regarded as homogeneous. In the second one, a more realistic picture of the adsorbent bed is used, taking into account its structure, made of several layers of activated carbon cloth. In both models, uniform conditions within the adsorbent particles (ACFC fibers) are assumed, i.e. both models can be regarded as macroscopic [4].

Both mathematical models are obtained as sets of coupled nonlinear partial and ordinary differential equations, defining the mass and heat balances in the system. The models also include expressions for calculation of the equilibrium and transport parameters.

The model equations are solved numerically. The PDEs are first approximated by larger sets of ordinary differential equations, using the method of orthogonal collocations [5]. The resulting sets of ODEs are further solved numerically, leading to the concentration and temperature profiles in time and space in the adsorber.

The obtained models are used for simulation of the processes of adsorption, electroresistive heating and electrothermal desorption, as well as consecutive adsorption-desorption, for a particular system.

3. Mathematical model of the single-cartridge adsorber with homogeneous adsorbent bed

In postulating this model it was assumed that the layers of the ACFC were coiled so tightly, that the contact between them was very intimate and the adsorbent density was uniform throughout the bed, so that the whole adsorbent bed could be treated as homogeneous.

The following additional assumptions were used in setting up this model:

- The mass and heat transfer resistances on the particle scale can be neglected.
- There are no changes of the concentrations and temperatures in the axial direction, i.e. only the gradients in the radial direction have to be taken into account, so that one-dimensional model can be used [4].
- Initially, the adsorbate concentrations in both phases are in equilibrium and uniform throughout the adsorbent bed (for the cases of adsorption and electroresistive heating without desorption, they are both 0). The temperatures of both phases are initially equal and uniform throughout the adsorbent bed.
- The fluid phase is an ideal gas mixture of the inert and the adsorbate (for the case of electroresistive heating without desorption, it is pure inert).
- The gas pressure is constant and uniform throughout the bed.
- Heat dispersion in the radial direction of the adsorbent bed, both in the solid and in the fluid phase, is taken into account.
- The gas in the inlet tube and in the space around the adsorbent bed is ideally mixed.
- All physical parameters and coefficients are considered as constants.
- The electric resistivity of the ACFC adsorbens is temperature dependent.
- The electric power is supplied under the constant voltage conditions during electroresistive heating and electrothermal desorption.

3.1. Mass and energy balances

Based on these assumptions, the mathematical model of the annular radial-flow adsorption bed presented in Fig. 3 was obtained by writing the material and energy balances for a differential element of the cartridge volume, as shown in Figure 4. By letting the thickness of this element Δr to zero, these balances are obtained as the following partial differential equations:

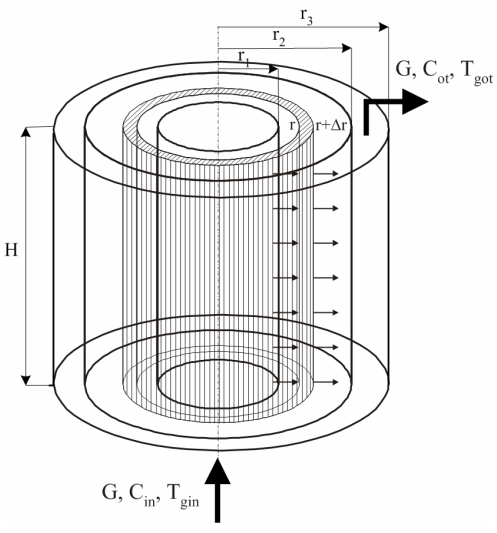

Figure 4 A differential volume element, used for modeling

Adsorbate balance for the solid phase within the adsorbent bed:

$$\rho_b \frac{\partial q}{\partial t} = (k_m a)(C - C^*) \qquad (1)$$

Adsorbate balance for the gas phase within the adsorbent bed:

$$\rho_g \frac{\partial C}{\partial t} + \frac{G}{(2r\pi H \varepsilon_b)} \frac{\partial C}{\partial r} + (k_m a)(C - C^*) = \frac{D_m}{r} \frac{\partial}{\partial r}\left(r \frac{\partial C}{\partial r} \right) \tag{2}$$

Heat balance for the solid phase within the adsorbent bed:

$$\rho_b \frac{\partial}{\partial t}\left[(c_{ps} + c_{pl} q) T_s \right] = \frac{\delta Q_{el}}{dV} + \Delta H_{ads} \rho_b \frac{\partial q}{\partial t} + \frac{D_t^{hs}}{r} \frac{\partial}{\partial r}\left(r \frac{\partial T_s}{\partial r} \right) - (ha)(T_s - T_g) \tag{3}$$

Heat balance for the gas phase within the adsorbent bed:

$$\begin{aligned} \rho_g \frac{\partial}{\partial t}\left[(c_{pg} + c_{pv} C) T_g \right] = & -\frac{G(c_{pg} + c_{pv} C)}{2r\pi H \varepsilon_b} \frac{\partial T_g}{\partial r} - \\ & \frac{G c_{pv} T_g}{2r\pi H \varepsilon_b} \frac{\partial C}{\partial r} + (ha)(T_s - T_g) + \frac{D_t^{hg}}{r} \frac{\partial}{\partial r}\left(r \frac{\partial T_g}{\partial r} \right) \end{aligned} \tag{4}$$

The *boundary conditions* for equations (1-4) are:

$$r=r_1: \quad D_m \left.\frac{\partial C}{\partial r}\right|_{r=r_1} = C - C_{it}, \quad D_t^{hs} \left.\frac{\partial T_s}{\partial r}\right|_{r=r_1} = h_{s1}(T_s - T_{git}), \quad D_t^{hg} \left.\frac{\partial T_g}{\partial r}\right|_{r=r_1} = h_{g1}(T_g - T_{git}) \tag{5}$$

$$r=r_2: \quad -D_m \left.\frac{\partial C}{\partial r}\right|_{r=r_2} = C - C_{ot}, \quad -D_t^{hs} \left.\frac{\partial T_s}{\partial r}\right|_{r=r_2} = h_{s2}(T_s - T_{got}), \quad -D_t^{hg} \left.\frac{\partial T_g}{\partial r}\right|_{r=r_2} = h_{g2}(T_g - T_{got}) \tag{6}$$

Using the assumption of ideal mixing in the central inlet tube and in the annular space around the adsorption bed (the outlet tube), the mass and heat balances for the gas phase in these two regions are obtained in the form of ordinary differential equation:

Adsorbate balance for the gas in the inlet tube:

$$r_1^2 \pi H \rho_g \frac{dC_{it}}{dt} = G C_{in} - G C_{it} + k_{m1}(2r_1\pi H)(1-\varepsilon_b)(C^*\big|_{r=r_1} - C_{it}) + 2r_1\pi H \varepsilon_b (C\big|_{r=r_1} - C_{it}) \tag{7}$$

Heat balance for the gas in the inlet tube:

$$\begin{aligned} r_1^2 \pi H \rho_g \frac{d}{dt}\left[(c_{pg} + c_{pv} C_{it}) T_{git} \right] = & G(c_{pg} + c_{pv} C_{in}) T_{gin} - G(c_{pg} + c_{pv} C_{it}) T_{git} \\ & + h_{s1}(2r_1\pi H)(1-\varepsilon_b)(T_{s|r=r_1} - T_{git}) + h_{g1}(2r_1\pi H \varepsilon_b)(T_{g|r=r_1} - T_{git}) \end{aligned} \tag{8}$$

Adsorbate balance for the gas in the outlet annular tube:

$$(r_3^2 - r_2^2)\pi H \rho_g \frac{dC_{ot}}{dt} = G\, C\big|_{r=r_2} - G C_{ot} + k_{m2}(2r_2\pi H)(1-\varepsilon_b)(C^*\big|_{r=r_2} - C_{ot}) + 2r_2\pi H \varepsilon_b (C\big|_{r=r_2} - C_{ot}) \tag{9}$$

Heat balance for the gas in the outlet annular tube:

$$\begin{aligned} & (r_3^2 - r_2^2)\pi H \rho_g \frac{d}{dt}\left[(c_{pg} + c_{pv} C_{ot}) T_{got} \right] = G(c_{pg} + c_{pv}\, C\big|_{r=r_2}) T_{g|r=r_2} - G(c_{pg} + c_{pv} C_{ot}) T_{got} \\ & + h_{s2}(2r_2\pi H)(1-\varepsilon_b)(T_{s|r=r_2} - T_{got}) + h_{g2}(2r_2\pi H \varepsilon_b)(T_{g|r=r_2} - T_{got}) - h_{wg}(2r_3\pi H)(T_{got} - T_a) \end{aligned} \tag{10}$$

The initial conditions for equations (1-4) and (7-10) are:

$$t<0,\ r\in[r_1,r_2]:\quad T_g=T_s=T_{git}=T_{got}=T_{gin}=T_{go}=T_a=T_p,\qquad C=C_{it}=C_{ot}=C_{in}=C^*=\Phi(q)=C_p \tag{11}$$

The notations of the main variables used in Figure 4 and equations (1-11) are: C – adsorbate concentration in the gas phase, q – adsorbate concentration in the solid phase, C^* - adsorbate concentration in the gas phase in equilibrium with the solid phase, T_g – gas temperature, T_s – solid temperature, t – time, r – the radial position in the cartridge, r_1 and r_2 – the inner and the outer diameter of the radial adsorbent bed, r_3 the diameter of the adsorber, H – the cartridge height, ε_b - bed porosity, G – molar flow-rate of the gas inert. The subscript *in* denotes the inlet, *o* the outlet, *it* the inlet tube, *ot* the outlet annular tube, *a* the ambient and *p* the previous (initial) state. δQ_{el} is the heat Joule heat generated in the differential element of volume. A complete list of the notations, including the physical parameters and coefficients used in these equations, can be found in the nomenclature, at the end of this report.

These model equations are valid for all three processes: adsorption, electroresistive heating and electrothermal desorption, assuming the proper definition of the variables (e.g. for adsorption $\delta Q_{el}=0$, $C_p=0$ and $C_{in}=\text{const}\neq 0$, for electroresistive heating $C_p=0$ and $C_{in}=0$, while for electrothermal desorption $C_p=\text{const}\neq 0$ and $C_{in}=0$).

3.2. Additional equations

For a complete mathematical model besides the balance equations and their initial and boundary conditions, it is necessary to define relations for calculating the equilibrium and transport parameters. A selection of these relations, based on literature, is given below.

Calculation of the equilibrium parameters (adsorption isotherm)

The equilibrium relation $C^*=\Phi(q)$ is one of the basic data needed for correct modeling of adsorption systems. In the presented model the Dubinin-Radushkevich equation was used, as it had been shown to describe reliably adsorption of organic vapors on ACFC [3]:

$$W = W_0 \exp\left(-\left(\frac{R_g T_s}{E}\ln\frac{p^o}{p_A}\right)\right) \tag{12}$$

In equation (13) W is the volume of the adsorbed phase per unite mass of adsorbent, W_0- the volume of the micropores per unit mass of adsorbent, E- the adsorbate energy of adsorption, p^o-the adsorbate saturation vapor pressure, p_A – the adsorbate partial pressure, T – temperature and R_g – the gas constant. The vapor pressure was calculated using the Wagner equation:

$$\ln\left(\frac{p^o}{p_c}\right)=\left(\frac{VP_A x+VP_B x^{1.5}+VP_C x^3+VP_D x^6}{1-x}\right) \tag{13}$$

where $x=1-(T_s/T_c)$, p_c and T_c are the critical pressure and temperature and VP_A, VP_B, VP_C and VP_D are Wagner constants.

Based on equation (12), the following relation between the equilibrium adsorbate concentration in the gas phase C^* and its concentration in the solid phase q and the temperature T_s, was obtained:

$$C^* = \frac{p^o}{p \exp\left[\frac{E}{R_g T_s}\sqrt{-\ln\left(\frac{M_A q}{\rho_A W_0}\right)}\right]} \tag{14}$$

(M_A and ρ_A are the adsorbate molar mass and density).

Depending on the particular system, another adsorption isotherm relation can be used, either based on theory or on experimental results.

Calculation of the transport parameters

The calculation of the main transport parameters was based on different correlations published in the literature. Most of the correlations used in this work are general, and do not correspond particularly to the fibrous structure of the adsorption bed. They could be replaced with more specific correlations, if they become available. Here are the procedures for calculation of the main transport parameters used in the model:

- *Heat transfer coefficient between the ACFC and the gas in the inlet or outlet tube h_{s1} and h_{s2}*

The criterial equation suggested in Ref. [13], was used for calculation of this heat transfer coefficient:

$$h_{s1/2} = \frac{Nu_H k}{H} \tag{15}$$

$$Nu_H = \left\{0.825 + \frac{0.387 Ra_H^{1/6}}{\left[1+(0.492/\mathrm{Pr})^{9/16}\right]^{8/27}}\right\}^2 \tag{16}$$

$$Ra_H = \frac{g\beta(T_s - T_\infty)H^3}{\alpha\nu} \tag{17}$$

$$\mathrm{Pr} = \frac{\mu(c_{pg} + c_{pv}C)}{k} \tag{18}$$

$$\alpha = \frac{k}{\rho_g (c_{pg} + c_{pv}C)} \tag{19}$$

In these equations, Nu_H is the Nuselt numper, Pr – the Prantl number, Ra_H - the Rayleigh number, k – the thermal conductivity of the gas phase, g – the gravity constant, β- the reciprocal value of the temperature of the film (approximately calculated as an arithmetic mean of the temperatures of the solid surface T_s and the bulk temperature of the gas T_∞), α - the thermal diffusivity and ν and μ - the kinematic and the dynamic viscosity of the gas phase, respectively.

- *Radial thermal conductivity of the gas phase within the adsorbent bed* D_t^{hg}

A correlation proposed by Edwards and Richardson [7] was used:

$$\frac{1}{Pe} = \frac{D_t^{hg}}{\rho_g v D_p (c_{pg} + c_{pv} C)} = \frac{0.73\varepsilon_b}{RePr} + \frac{0.5}{1 + (9.7\varepsilon_b)/(RePr)} \tag{20}$$

$$Re = \frac{\rho_g v D_p}{\mu} \tag{21}$$

$$v = \frac{G}{2r\pi H \rho_g} \tag{22}$$

where Pe is the Peclet number, Re – the Reynolds number, D_p – the particle diameter and v – the superficial gas velocity. The value of the Pe number changes with time and the radial position in the bed, while the superficial velocity, and consecutively, the Re number changes with the radial position in the bed. Accordingly, the radial thermal diffusivity is a function of both time and the radial position in the adsorbent bed.

- *Gas to solid mass transfer coefficient in the ACFC adsorbent bed* k_m

This coefficient was calculated using the following criterial equation [6]:

$$Sh = 0.91\Psi \,\mathrm{Re}^{0.49}\, Sc^{1/3} \tag{23}$$

$$Sc = \frac{\mu}{\rho_g D_{AB}} \tag{24}$$

$$Sh = \frac{k_m D_p}{D_{AB}} \tag{25}$$

where Sh is the Sherwood number, Sc – the Schmidt number, D_{AB} – the molecular diffusivity of the adsorbate in the gas inert and Ψ - the shape factor (0.81 for cylindrical particles).

The molecular diffusivity D_{AB} was calculated using the Chapman-Enskog correlation [6]:

$$D_{AB} = \frac{0.001858 T_g^{3/2} \sqrt{\dfrac{M_A + M_B}{2 M_A M_B}}}{P \sigma_{AB}^2 \Omega_D} \tag{26}$$

with: $\sigma_{AB} = \dfrac{\sigma_A + \sigma_B}{2}$ - the characteristic length of the binary pair

$\sigma = 2.44\,(T_c/P_c)^{1/3}$ - the characteristic length of a single molecule

$\Omega_D = \left(44.54 T^{*-4.909} + 1.911 T^{*-1.575}\right)^{0.10}$ - the collision integral

$T^* = k_b T_g / \varepsilon_{AB}$

$\varepsilon_{AB} = (\varepsilon_A \varepsilon_B)^{1/2}$

ε_A – the characteristic Lennard -Jones energy

$\varepsilon / k = 0.75 T_c$

k_b - Boltzmann's constant

- *Gas to solid heat transfer coefficient in the ACFC adsorbent bed h*:

Based on the analogy between mass and heat transfer in the adsorbent bed [6, 9], a criterial equation analogous to equation (25) was used:

$$Nu = 0.91 \Psi \, \mathrm{Re}^{0.49} \, \mathrm{Pr}^{1/3} \tag{27}$$

- *Radial mass dispersion coefficient in the gas phase D_m*

Based on the analogy between mass and heat transfer [9] and the equation for the heat dispersion coefficient, the following was used:

$$D_m = \frac{D_t^{hg}}{(c_{pg} + c_{pv} C)} \tag{28}$$

Calculation of the Joule heat

An important term, differentiating electroresistive heating from other processes, is $\delta Q_{el}/dV$, in equation (3). It represents the Joule heat generated in a unit bed volume. For the case of constant electric voltage supply, this term can be derived through the following steps:

- Calculation of the specific electric resistivity of ACFC, which is temperature dependent. A linear relationship, suggested in Ref. [3] was used:

$$\rho = f(T_s) = \left(\rho_0 (1 + b(T_s - T_R))\right) = f(r,t) \tag{29}$$

where ρ_0 is the electric resistivity at the referent temperature T_R and b is the temperature coefficient of the electric resistivity.

- Calculation of the electric resistance of the differential volume element defined in Fig.4 ($dV = 2r\pi H dr$):

$$dR_{el}(r,t) = \frac{\rho(T_s) H}{dA} = \frac{\rho(T_s) H}{2r\pi dr} \tag{30}$$

- Calculation of the electric current through the differential volume element dV, under constant voltage conditions:

$$dI(r,t) = \frac{U}{dR_{el}(r,t)} = \frac{2r\pi U dr}{\rho(T_s) H} \tag{31}$$

- Calculation of the Joule heat generated in the differential volume element dV:

$$\delta Q_{el} = U dI(r,t) = \frac{2r\pi U^2 dr}{\rho(T_s) H} \tag{32}$$

- Calculation of the heat generated per unite volume:

$$\frac{\delta Q_{el}}{dV} = \frac{U^2}{\rho(T_s) H^2} \tag{33}$$

The electric resistivity $\rho(T_s)$ is calculated for the local value of the solid phase temperature. As this temperature varies both with time and with the radial position in the bed, so does the Joule heat supplied to the element of the volume in question.

3.3. Numerical solution of the model equations

The first step of the numerical solution was approximation of the partial differential equations (1-4) by a larger set of ordinary differential equations, by applying the method of orthogonal collocation [5]. Before applying this method, the radial coordinate of the adsorption bed was transformed into a nondimensional one, using the following relation:

$$u = \frac{r - r_1}{r_2 - r_1} \tag{34}$$

Figure 5 gives a schematic representation of the distribution of the collocation points in the bed. N internal collocation points were used, plus the border points u=0 (r=r_1) and u=1 (r=r_2).

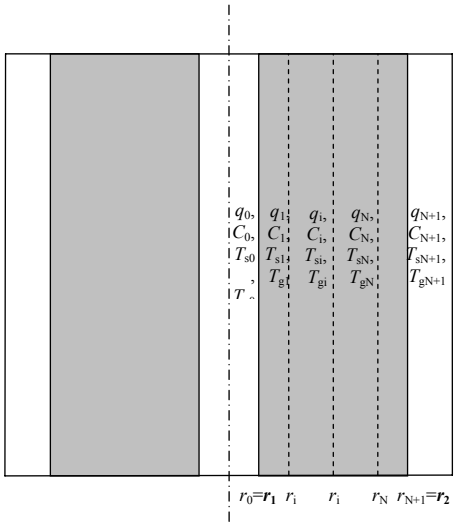

Figure 5 Schematic representation of the distribution of the collocation points

Here are the resulting equations:

$$\frac{dq_i}{dt} = \frac{k_m a}{\rho_b}(C_i - C_i^*), \quad i=0,...,N+1 \tag{35}$$

$$\frac{dC_i}{dt} = -\frac{G\sum_{j=0}^{N+1} A_{ij} C_j}{2\pi H \varepsilon_b \rho_g \Delta(\Delta u_i + r_1)} - \frac{k_m a}{\rho_g}(C_i - C_i^*) + \frac{D_m \sum_{j=0}^{N+1} B_{i,j} C_j}{(\Delta u + r_1)\rho_g} \qquad i=1,...,N+1 \tag{36}$$

$$\frac{dT_{si}}{dt} = \frac{\delta Q_i}{dV \rho_b (c_{ps} + c_{pl} q_i)} + \frac{(\Delta H_{ads} - c_{pl} T_{si})\rho_b \frac{dq_i}{dt} - (ha)(T_{si} - T_{gi})}{\rho_b (c_{ps} + c_{pl} q_i)} + \frac{D_t^{hs}}{(u_i \Delta + r_1)\rho_b (c_{ps} + c_{pl} q)} \sum_{j=0}^{N+1} B_{i,j} T_{sj}, \tag{37}$$

$$i=1,...,N$$

$$\frac{dT_{gi}}{dt} = \frac{(ha)(T_{si} - T_{gi})}{\rho_g (c_{pg} + c_{pv} C_i)} - \frac{G\sum_{j=0}^{N+1} A_{ij} T_{gj}}{2\pi H \varepsilon_b \rho_g \Delta(u_i \Delta + r_1)} - \frac{G c_{pv} T_{gi} \sum_{j=0}^{N+1} A_{ij} C_j}{2\pi H \varepsilon_b \rho_g \Delta(u_i \Delta + r_1)(c_{pg} + c_{pv} C_i)}, \tag{38}$$

$$- \frac{c_{pv} T_{gi} \frac{dC_i}{dt}}{(c_{pg} + c_{pv} C_i)} + \frac{D_t^{hg}}{(u_i \Delta + r_1)\rho_g (c_{pg} + c_{pv} C_i)} \sum_{j=0}^{N+1} B_{i,j} T_{gj}, \qquad i = 1,..., N$$

The mass and heat balances for the inlet and outlet gas tubes were also rearranged:

$$\frac{dC_{it}}{dt} = \frac{G(C_{in} - C_{it})}{r_1^2 \pi H \rho_g} + \frac{k_{m1}(2r_1 \pi H)(1 - \varepsilon_b)(C_0^* - C_{it})}{r_1^2 \pi H \rho_g} + \frac{2r_1 \pi H \varepsilon_b (C_0 - C_{it})}{r_1^2 \pi H \rho_g} \tag{39}$$

$$\frac{dT_{git}}{dt}=\frac{G(c_{pg}+c_{pv}C_{in})T_{gin}}{r_1^2\pi H\rho_g(c_{pg}+c_{pv}C_{it})}-\frac{GT_{git}}{r_1^2\pi H\rho_g}+\frac{h_{s1}(2r_1\pi H)(1-\varepsilon_b)(T_{s0}-T_{git})}{r_1^2\pi H\rho_g(c_{pg}+c_{pv}C_{it})}+$$
$$\frac{h_{g1}(2r_1\pi H\varepsilon_b)(T_{g0}-T_{git})}{r_1^2\pi H\rho_g(c_{pg}+c_{pv}C_{it})}-\frac{c_{pv}T_{git}}{(c_{pg}+c_{pv}C_{it})}\frac{dC_{it}}{dt} \quad (40)$$

$$\frac{dC_{ot}}{dt}=\frac{G(C_{N+1}-C_{ot})}{(r_3^2-r_2^2)\pi H\rho_g}+\frac{k_{m2}(2r_2\pi H)(1-\varepsilon_b)(C_{N+1}^*-C_{ot})}{(r_3^2-r_2^2)\pi H\rho_g}+\frac{2r_2\pi H\varepsilon_b(C_{N+1}-C_{ot})}{(r_3^2-r_2^2)\pi H\rho_g} \quad (41)$$

$$\frac{dT_{got}}{dt}=\frac{G(c_{pg}+c_{pv}C_{N+1})T_{gN+1}}{(r_3^2-r_2^2)\pi H\rho_g(c_{pg}+c_{pv}C_{ot})}-\frac{GT_{got}}{(r_3^2-r_2^2)\pi H\rho_g}+\frac{h_{s2}(2r_2\pi H)(1-\varepsilon_b)(T_{sN+1}-T_{got})}{(r_3^2-r_2^2)\pi H\rho_g(c_{pg}+c_{pv}C_{ot})}+$$
$$\frac{h_{g2}(2r_2\pi H\varepsilon_b)(T_{gN+1}-T_{got})}{(r_3^2-r_2^2)\pi H\rho_g(c_{pg}+c_{pv}C_{ot})}-\frac{h_{wg}(2r_3\pi H)(T_{got}-T_a)}{(r_3^2-r_2^2)\pi H\rho_g(c_{pg}+c_{pv}C_{ot})}-\frac{c_{pv}T_{got}}{(c_{pg}+c_{pv}C_{ot})}\frac{dC_{ot}}{dt} \quad (42)$$

The boundary conditions (6-7) are also transformed into the following algebraic expressions:

$$C_0=\frac{C_{it}+D_m\frac{1}{\Delta}\sum_{j=1}^{N+1}A_{o,j}C_j}{1+D_m\frac{1}{\Delta}A_{0,0}},\quad T_{g0}=\frac{h_{g1}T_{git}+D_t^{hg}\frac{1}{\Delta}\sum_{j=1}^{N+1}A_{o,j}T_{gj}}{h_{g1}+D_t^{hg}\frac{1}{\Delta}A_{0,0}},\quad T_{s0}=\frac{h_{s1}T_{git}+D_t^{hs}\frac{1}{\Delta}\sum_{j=1}^{N+1}A_{o,j}T_{sj}}{h_{s2}+D_t^{hs}\frac{1}{\Delta}A_{0,0}} \quad (43)$$

$$C_{N+1}=\frac{C_{ot}-D_m\frac{1}{\Delta}\sum_{j=0}^{N}A_{N+1,j}C_j}{1+D_m\frac{1}{\Delta}A_{N+1,N+1}},\quad T_{sN+1}=\frac{h_{s2}T_{got}-D_t^{hs}\frac{1}{\Delta}\sum_{j=o}^{N}A_{N+1,j}T_{sj}}{h_{s2}+D_t^{hs}\frac{1}{\Delta}A_{N+1,N+1}},\quad T_{gN+1}=\frac{h_{g2}T_{got}-D_t^{hg}\frac{1}{\Delta}\sum_{j=0}^{N}A_{N+1,j}T_{gj}}{h_{g2}+D_t^{hg}\frac{1}{\Delta}A_{N+1,N+1}} \quad (44)$$

$A_{i,j}$ and $B_{i,j}$ are the first and second order derivatives of the Lagrangian polynomials l_j used in the method of orthogonal collocations [5]:

$$A_{i,j}=\left(\frac{dl_j}{du}\right)_{u=u_i},\qquad B_{i,j}=\frac{u_i\Delta+r_1}{\Delta^2}\left(\frac{d^2l_j}{du^2}\right)_{u=u_i}+\frac{1}{\Delta}\left(\frac{dl_j}{du}\right)_{u=u_i} \quad (45)$$

($\Delta=r_2-r_1$ is the bed thickness.)

Equations (35-42) represent a set of $4N+6$ nonlinear ODEs which, together with 6 algebraic equations, define the concentrations and temperatures in the solid and in the gas phase in all collocation points of the annular adsorption bed, as well as in the gas phase in the inlet and in the outlet tube. This set of equations was solved numerically, using the Matlab function *ode15s*.

The derived model was used for simulation of the concentration and temperature profiles of both phases in different points of the ACFC, as well as in the inlet and outlet tube, for 3 different processes: adsorption on an initially clean ACFC bed, electroresistive heating of a clean ACFC bed and electrothermal desorption from a previously saturated ACFC bed. The parameters used for simulation are listed in Table 1. They correspond to the experimental system defined in Ref. [3]: methyl ethyl ketone (MEK) as adsorbate, American Kynol ACC-5092-20 as adsorbent and nitrogen as carrier gas. The equilibrium and most of the transport parameters were calculated using the expressions given in Section 3.2, while for the rest, arbitrary values, given in Table 1, were used.

Table 1. Parameter values used for simulation of adsorption, electroresistive heating and electrothermal desorption, using the model of a homogeneous adsorption bed

Variable	Notation and value
Inner diameter of the cartridge	r_1=0.95 cm
Outer diameter of the outlet annular tube	r_3=3.55 cm
Bed thickness	$\Delta=r_2-r_1$=0.55 cm
Bed axial dimension	H=30 cm
Bed porosity	ε_b=0.72
Particle (fiber) diameter	$D_p=13\times10^{-4}$ cm
Specific surface area	a=13.65 cm^2/cm^3
Gas pressure	p=101325 Pa
Inlet adsorbate concentration in the gas phase during adsorption	C_{in}=0.001 mol/mol
Inlet adsorbate concentration in the gas phase during desorption	C_{in}=0 mol/mol
Initial adsorbate concentration in the solid phase for desorption	q_p=0.003 mol/g
Inlet gas temperature	T_{gin}=293.15 K
Ambient temperature	T_a=293.15 K
Mass transfer coefficient in bed	k_m=0.0003 mol/(cm^{2}s)
Mass transfer coefficient from the solid phase to the gas phase in the inlet tube	k_{m1}=0.0003 mol/(cm^{2}s)
Mass transfer coefficient from the solid phase to the gas phase in the outlet annular tube	k_{m2}=0.0003 mol/(cm^{2}s)
Solid to gas heat transfer coefficient	$h=9\times10^{-4}$ W/(cm^{2}K)
Heat transfer coefficient from the gas phase in bed to the gas phase in the inlet tube	$h_{g1}=8\times10^{-3}$ W/(cm^{2}K
Heat transfer coefficient from the gas phase in bed to the gas phase in the outlet annular tube	$h_{g2}=2\times10^{-3}$ W/(cm^{2}K
Gas to ambient heat transfer coefficient (heat losses)	$h_{wg}=5\times10^{-6}$ W/(cm^{2}K)
Heat diffusivity of the solid phase	$D_t^{hs}=1.2\times10^{-4}$ W/(cmK)
Heat of adsorption	ΔH_{ads}=66200 J/mol
Adsorbent bed density	ρ_b=0.221 g/cm^3
Density of the inert gas	ρ_g=0.000416 mol/cm^3
Adsorbate density	ρ_A=0.81 g/cm^3
Adsorbate molar mass	M_A=72.107 g/mol
Inert gas molar mass (nitrogen)	M_B=28.02 g/mol
Specific heat capacity of liquid adsorbate	c_{pl}=157.9 J/(molK)
Specific heat capacity of the inert gas	c_{pg}=29.13 J/(molK)
Heat capacity of the solid phase	c_{ps}=0.71 J/(gK)
Specific heat capacity of gaseous adsorbate	c_{pv}=100.9 J/(molK)
Dynamic viscosity of the inert gas	$\mu=1.78\times10^{-4}$ g/cm/s
Inert gas thermal conductivity	$k=2.6\times10^{-4}$ W/cm/K
Referent temperature	T_R=293.15 K
Critical temperature of the adsorbate	T_{cA}=536.8 K
Critical temperature of the inert gas (nitrogen)	T_{cB}=126.2 K
Critical pressure of the adsorbate	$p_{cA}=4.26\times10^{+6}$ Pa
Critical pressure of the inert gas (nitrogen)	$p_{cB}=3.39\times10^{+6}$ Pa

Wagner constants for the adsorbate	VP_A=-7.71476 VP_B=1.71061 VP_C=-3.6877 VP_D=-0.75169
Total volume of micropores (D-R equation)	W_0=0.748 cm^3/g
Gas constant	R_g=8.314 J/(molK)
Gravitation constant	g=9.81×10^2 cm/s^2
Boltzmann's constant	k_b=1.38048×10^{-23} J/K
Adsorption energy of the adsorbate (D-R eq.)	E=14.43×10^{+3} J/mol
Electric resistivity at referent temperature T_R	ρ_0=0.202 Ωcm
Temperature coefficient of the bed electrical resistivity	b=1.02e^{-5} 1/T

3.4. Simulation of adsorption

An important step of the TSA process is the adsorption part. Using the model presented here, simulation of adsorption on a previously clean ACFC bed, for constant inlet gas concentration and temperature, was performed. For this case, the model equations were solved for the following conditions: δQ_{el}=0, C_p=0, T_p=const, C_{in}=const, T_{in}=const.

Some of the simulation results obtained for the parameter values given in Table 1 and for 10 collocation points (N+2=10) are shown in Figures 6-9.

Figures 6 and 7 show the space and time distributions of the concentrations (Fig. 6) and temperatures (Fig. 7) in the solid (figs (a)) and in the gas phase (figs (b)). In these figures, lines of different colors correspond to different collocation points in the bed, the distribution of which is shown in the figures as well, by colored dots (e.g. the red lines and red dots correspond to the inner boundary point r=r_1, while the gray ones correspond to the outer boundary point r=r_2). The concentrations and temperatures of the gas phase in the inlet and in the outlet tube are also shown, as dashed black lines. For the parameters used, these lines overlap with the border lines corresponding to the gas phase in the adsorption bed.

Figures 6 and 7 actually show the propagation of the concentration and temperature fronts in the radial direction of the bed.

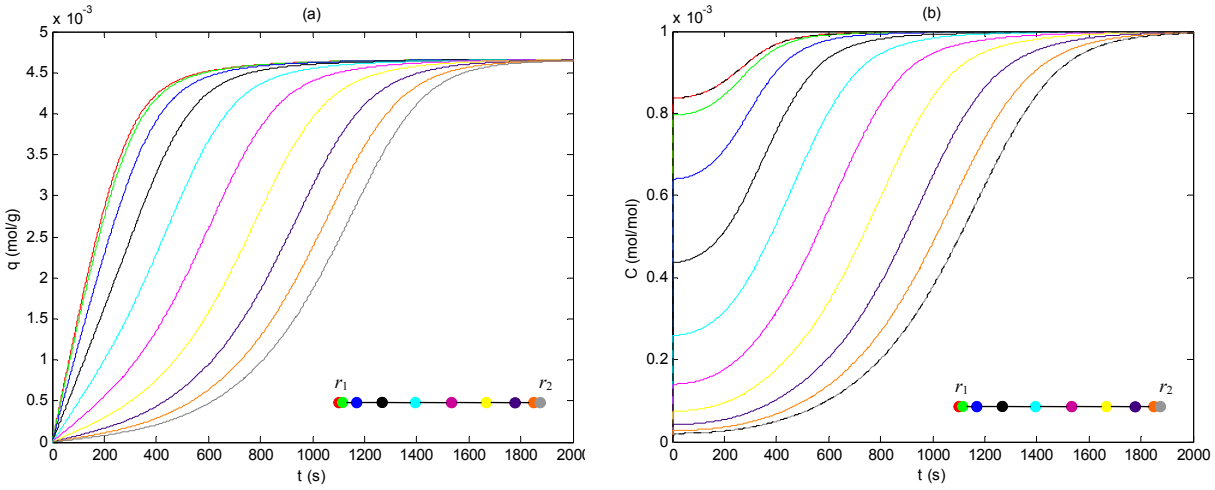

Figure 6 Simulation of adsorption - time profiles of the concentrations in 10 collocation points in the ads. bed (colored lines) and in the inlet and outlet tubes (---), for G=0.1 mol/s : a) Solid phase; b) Gas phase

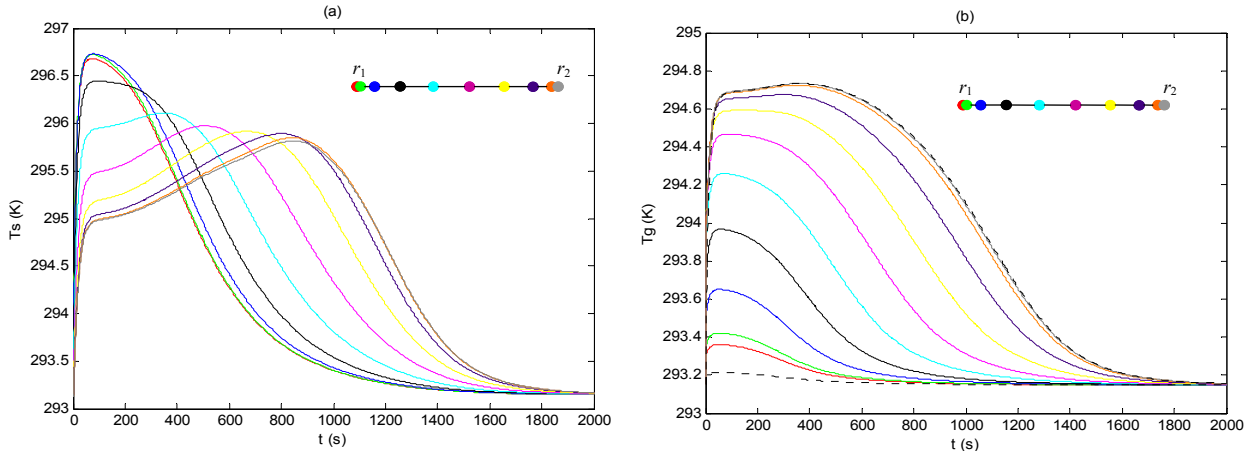

Figure 7 Simulation of adsorption - time profiles of the tempaeratures in 10 collocation points in the ads. bed (colored lines) and in the inlet and outlet tubes (---), for G=0.1 mol/s : a) Solid phase; b) Gas phase

The simulation was also used to investigate the influence of the inert gas flow-rate on the adsorption results. The simulated concentrations in the solid phase at the outer surface of the adsorption bed (for r=r_2) and in the outlet gas streams, obtained for 3 different flow-rates, are shown in Figures 8(a) and 8(b), and the corresponding temperatures, in Figures 9(a) and 9(b).

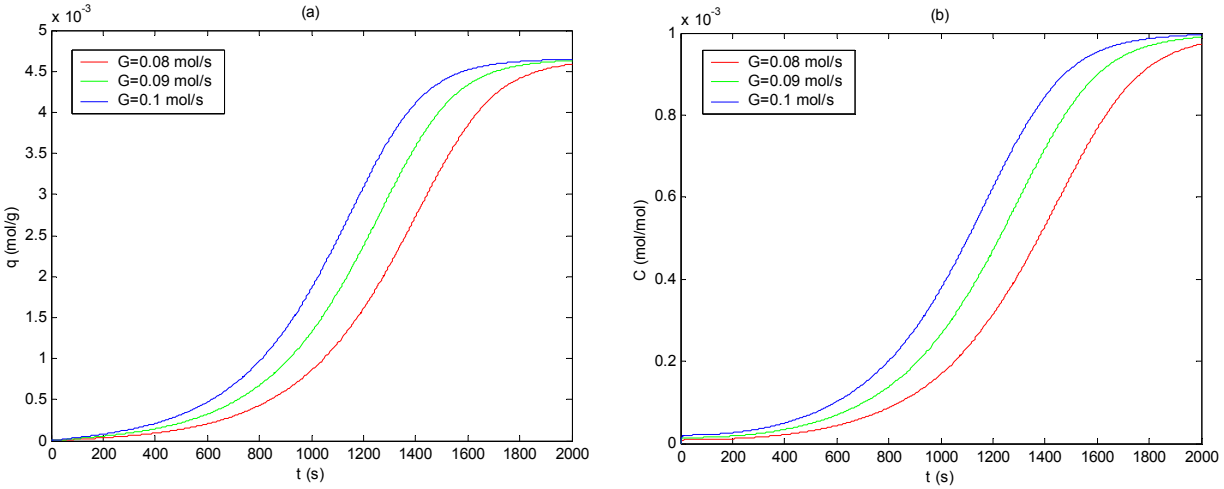

Figure 8. Simulation of adsorption – influence of the gas flow-rate on the concentrations:
a) Concentration in the solid phase at r=r_2, b) Outlet gas concentration

It has to be mentioned that the expressions for calculation of the mass and heat transfer parameters k_m and h, presented in Section 3.2. could not be used in these simulations, as they gave values which caused serious convergence problems. The values given in Table 1 were used instead. The calculated values of h were used only for simulation of electroresistive heating.

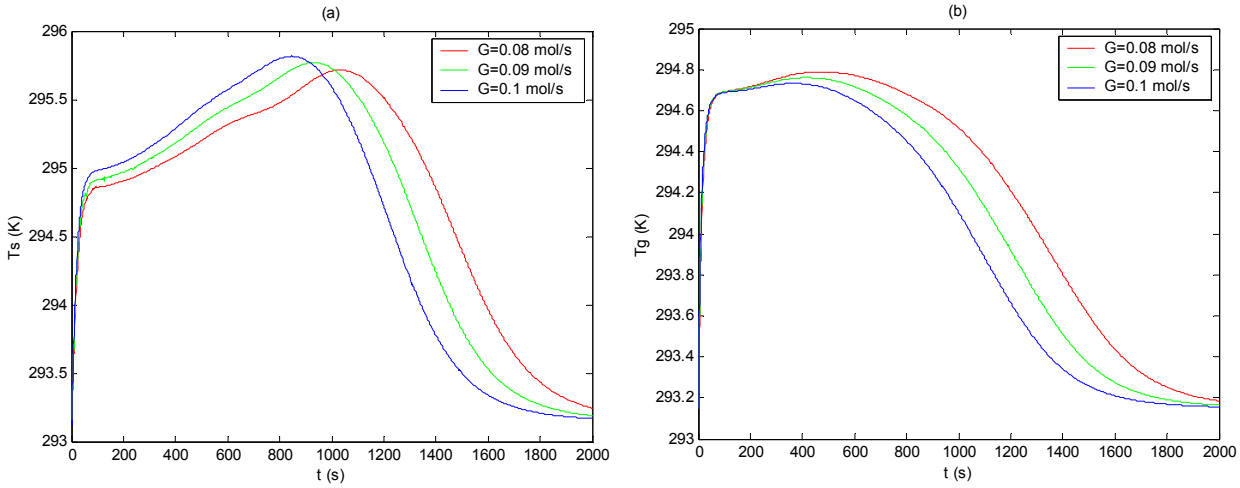

Figure 9. Simulation of adsorption – influence of the gas flow-rate on the temperatures:
a) Temperature of the solid at $r=r_2$, b) Outlet gas temperature

3.5. Simulation of electroresistive heating

In order to get a reliable description of the electrothermal desorption process, it is important to correctly model pure electroresistive heating of an adsorbate-free bed, first. This model would enable to predict the temperature profiles in the bed. Having some experimental measurements of the temperatures would enable estimation of the parameters defining the heat generation and heat transfer separately, and using them in modeling of electrothermal desorption.

The model presented in Section 3.1 can as well be used for electroresistive heating, assuming that Joule heat is generated inside the solid phase and that both the gas and the solid phase are adsorbate-free at all times: $\delta Q_{el}\neq 0$, $C_p=0$, $T_p=$const, $C_{in}=0$, $T_{in}=$const. Accordingly, all material balance equations and their appropriate boundary conditions can be omitted, and the solid and gas heat balances for the adsorption bed, together with the heat balances for the inlet and the outlet tube, can be solved separately. After applying the method of orthogonal collocations, the model reduces to $2N+2$ ODEs and 4 algebraic equations.

The simulation results presented here (in Figures 10-12) were obtained for constant electric voltage supply. Ten collocation points ($N+2=10$) were used for numerical solution of the PDEs. The simulated time profiles of the solid and gas temperatures in different collocation points in the bed are shown in Figure 10, as colored lines, and the gas temperatures in the inlet and in the outlet tube as black dashed lines. The influence of the gas flow-rate is shown in Figure 11, and the influence of the applied electrical voltage in Figure 12. In these two figures, the simulated time profiles of the outlet gas temperature and the solid temperature at the outer surface of the cartridge are shown.

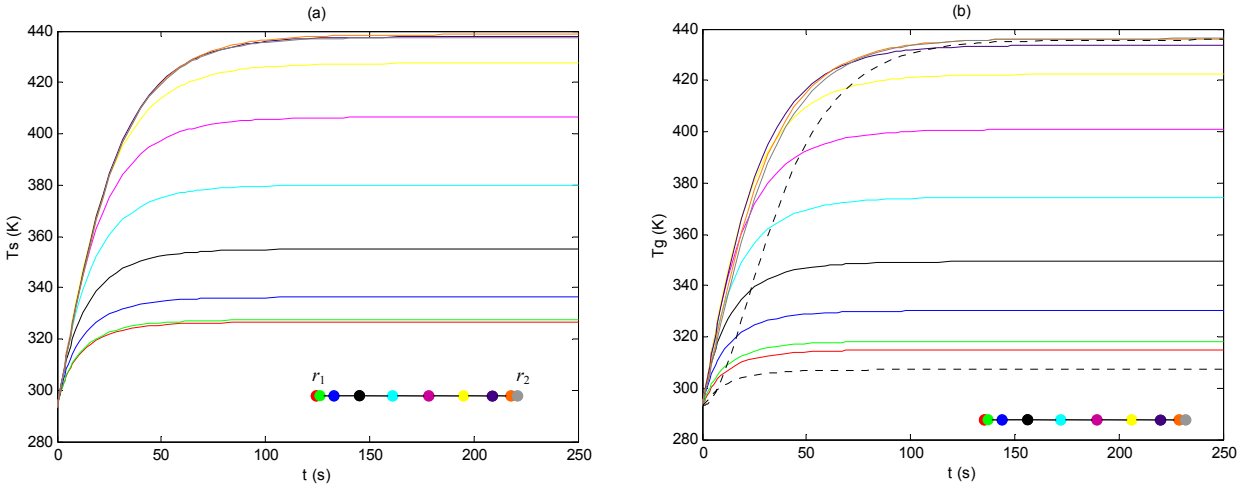

Figure 10 Simulation of electroresistive heating - time profiles of the temperatures in 10 collocation points in the ads. bed (colored lines) and in the inlet and outlet tubes (---), for G=0.02 mol/s and U=12 V : a) solid phase, b) gas phase

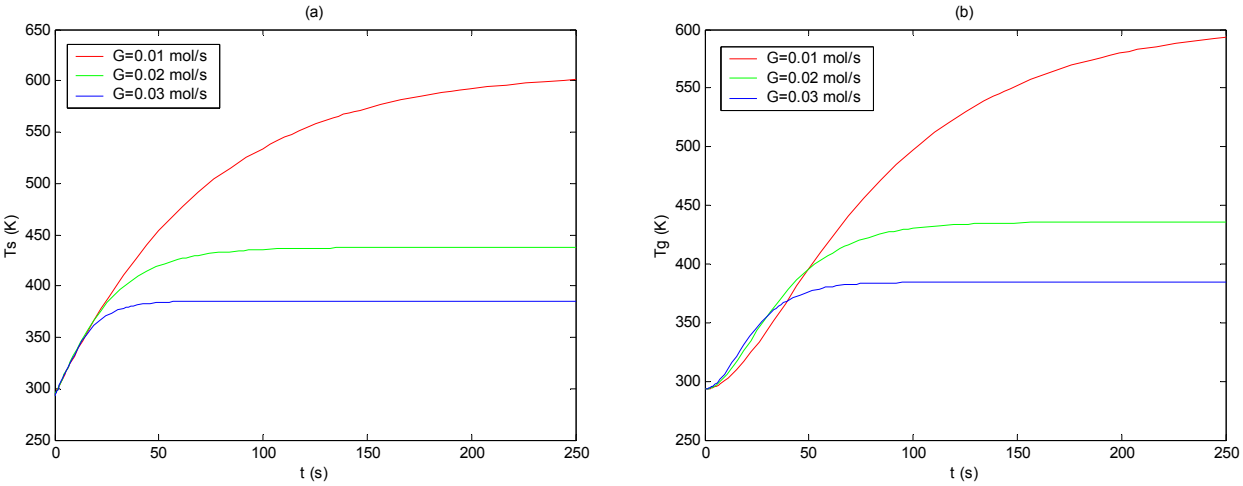

Figure 11 Simulation of electroresistive heating – influence of the gas flow-rate on the temperatures for U=12 V: a) Temperature of the solid at r=r_2, b) Outlet gas temperature

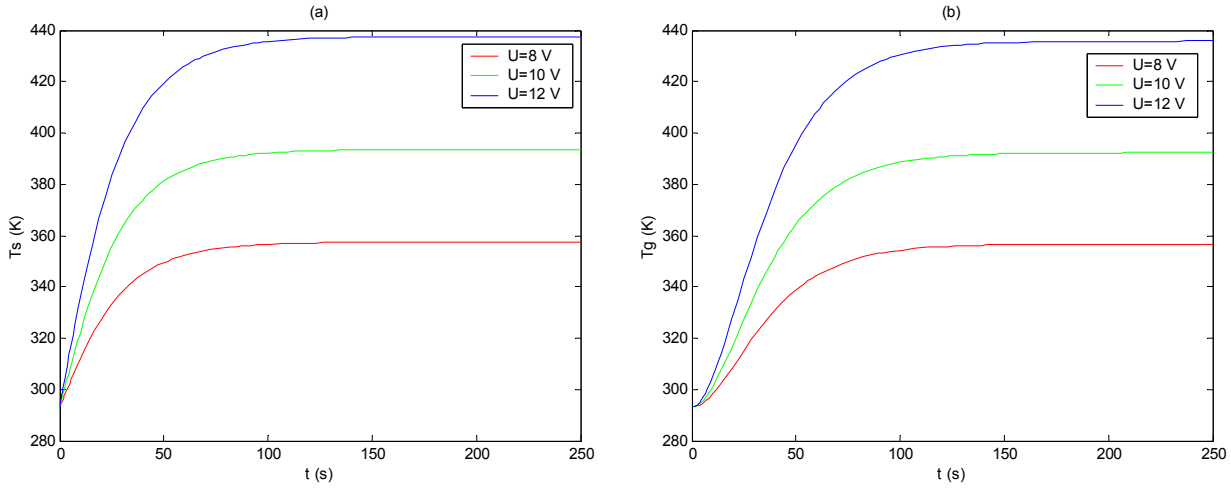

Figure 12 Simulation of electroresistive heating – influence of the electric voltage on the temperatures for G=0.02 mol/s: a) Temperature of the solid at r=r_2, b) Outlet gas temperature

3.6. Simulation of electrothermal desorption

In electrothermal desorption, a previously adsorbed adsorbate is desorbed owing to Joule heat generated inside the adsorbent material and a flow of pure inert through the adsorbent bed. The model developed in Section 3.1 was used for simulation of electrothermal desorption, for the case of thermal and concentration equilibrium and uniform concentration and temperature distributions in the adsorbent bed in the initial state, and for constant electric voltage supply during electrothermal desorption (C_p=const≠0,T_p=const, C_{in}=0, T_{gin}=const and U=const).

Some of the simulation results obtained with 10 collocation points are shown in 13-16. The time profiles in different collocation points in the adsorption bed and in the inlet and outlet tubes) are shown in Figure 13 (concentrations q and C) and Figure 14 (temperatures T_s and T_g). Figure 15 illustrates the influence of the gas flow-rate, and Figure 16 the influence of the applied voltage on the concentrations and temperatures corresponding to the outer boundary of the adsorbent bed and the outlet gas stream.

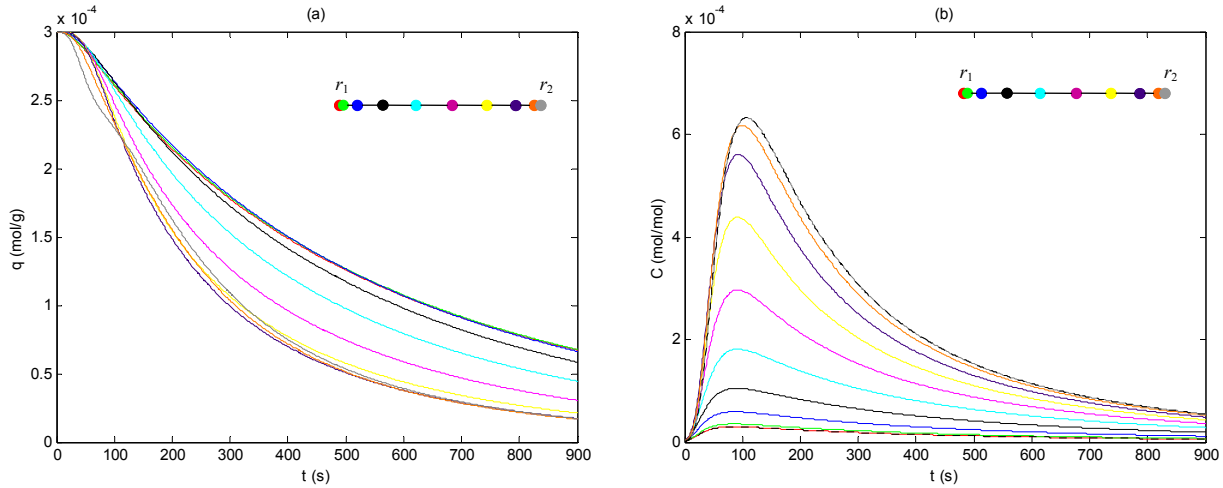

Figure 13 Simulation of electrothermal desorption - time profiles of the concentrations in 10 collocation points in the ads. bed (colored lines) and in the inlet and outlet tubes (---), for G=0.03 mol/s and U=10 V: a) solid phase; b) gas phase

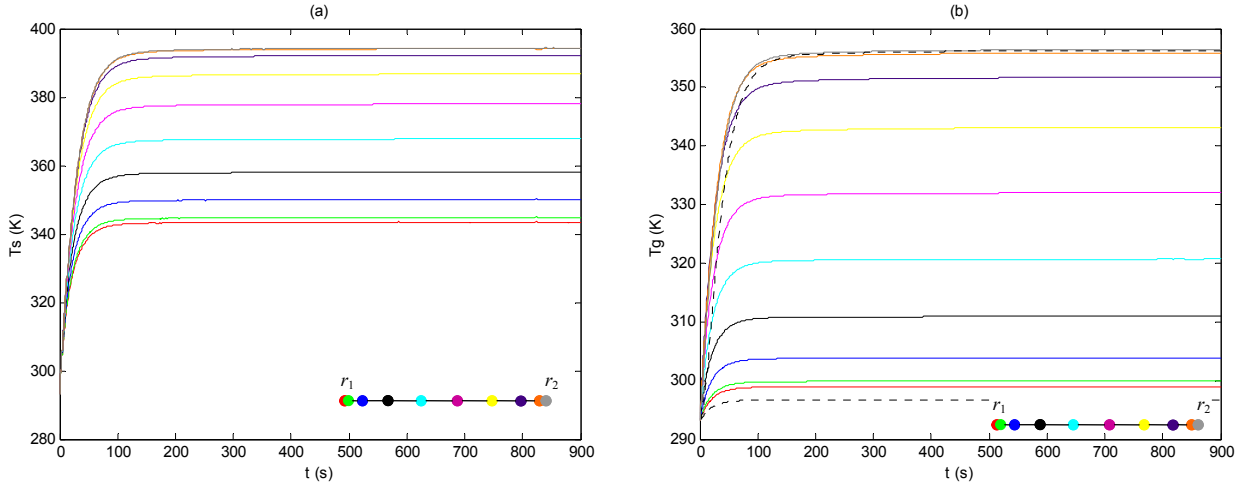

Figure 14 Simulation of electrothermal desorption - time profiles of the temperature in 10 collocation points in the ads. bed (colored lines) and in the inlet and outlet tubes (---), for G=0.03 mol/s and U=10 V: a) solid phase; b) gas phase

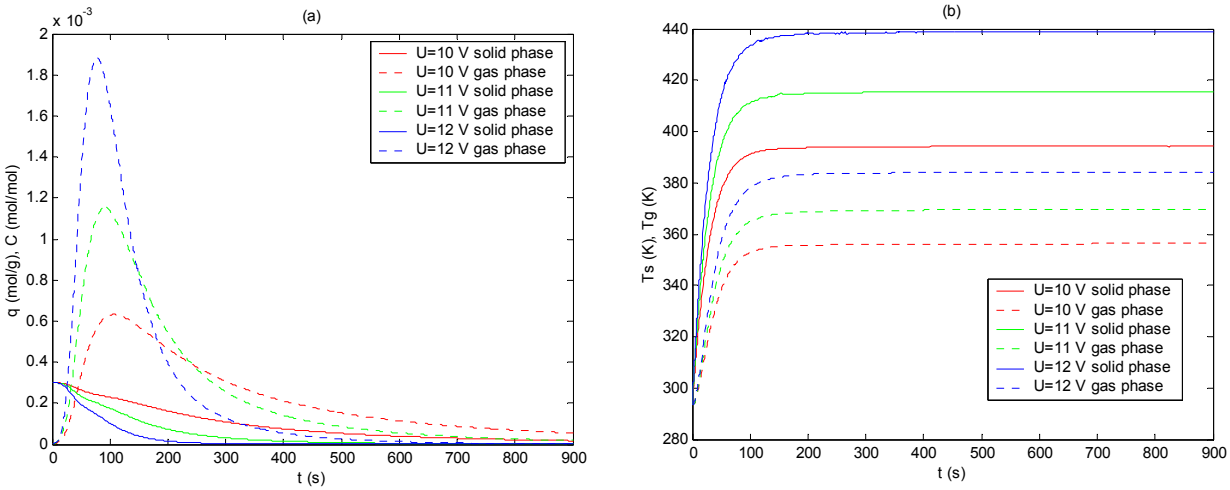

Figure 15 Simulation of electrothermal desorption – influence of the electric voltage on concentrations and temperatures at $r=r_2$ (solid) and in the outlet tube (gas) for G=0.03 mol/s: a) Concentrations and b) Temperatures

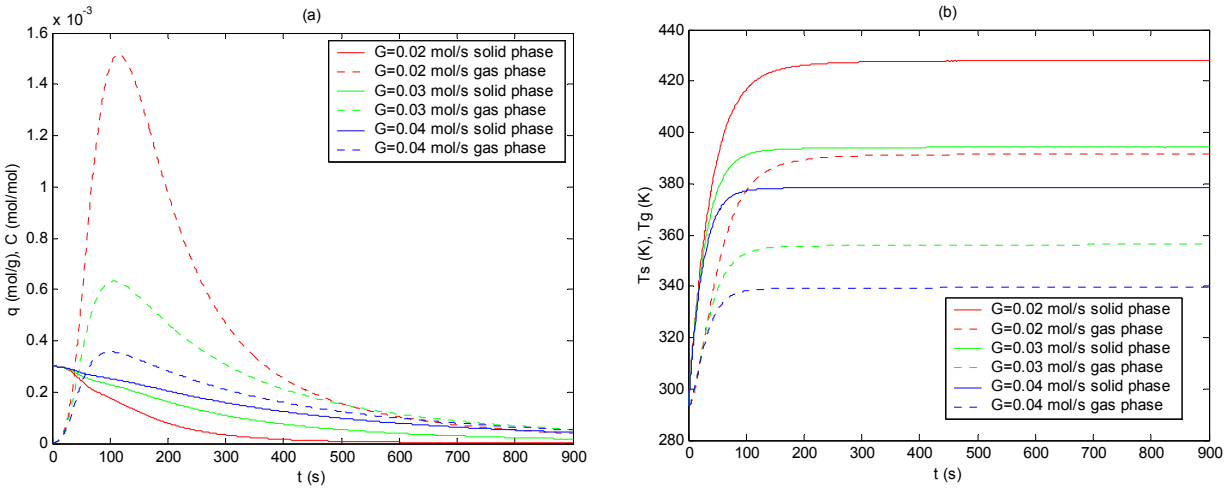

Figure 16 Simulation of electrothermal desorption – influence of the electric voltage on concentrations and temperatures at $r=r_2$ (solid) and in the outlet tube (gas) for G=0.03 mol/s: a) Concentrations and b) Temperatures

.

3.7 Simulation of consecutive adsorption-desorption

The TSA process with electrothermal desorption step consists of consecutive adsorption and desorption steps. The model defined in Section 3.1 was used for simulation of one cycle of consecutive adsorption-desorption, i.e., adsorption during the first part of the process, followed by electrothermal desorption under constant voltage supply and with flow of pure innert. This process can be defined by the following initial conditions:

$t<0$: $T_g=T_s=T_{git}=T_{got}=T_{gin}=T_{go}=T_a=T_p$, $C=C_{it}=C_{ot}=C_{in}=C^*=\Phi(q)=C_p=0$

and the following time changes of the inlet concentration, voltage and inert flow-rate:

$0\le t\le t_s$: C_{in}=const≠0, U=0 (δQ_{el}=0), $G=G_{ADS}$ - adsorption step

$t>t_s$: C_{in}=0, U=const≠0 (δQ_{el}≠0), $G=G_{ED}$ – electrothermal desorption step

Some of these simulation results are shown in Figures 17-20. In these simulations the switching time between adsorption and desorption t_s was chosen as the breakthrough time, i.e. the time after which the outlet concentration reached 5% of the inlet concentration. As in the real TSA process [3], the flow-rate during desorption was much lower than during the adsorption step. The presented results were again obtained for 10 collocation points.

The time profiles of the concentrations in both phases in all collocation points, as well as the gas phase in the inlet and in the outlet tube are shown in Figure 17, and the corresponding temperatures in Figure 18. The influence of the electrical voltage during the desorption step is shown in Figure 19, and the influence of the flow-rate during desorption in Figure 20.

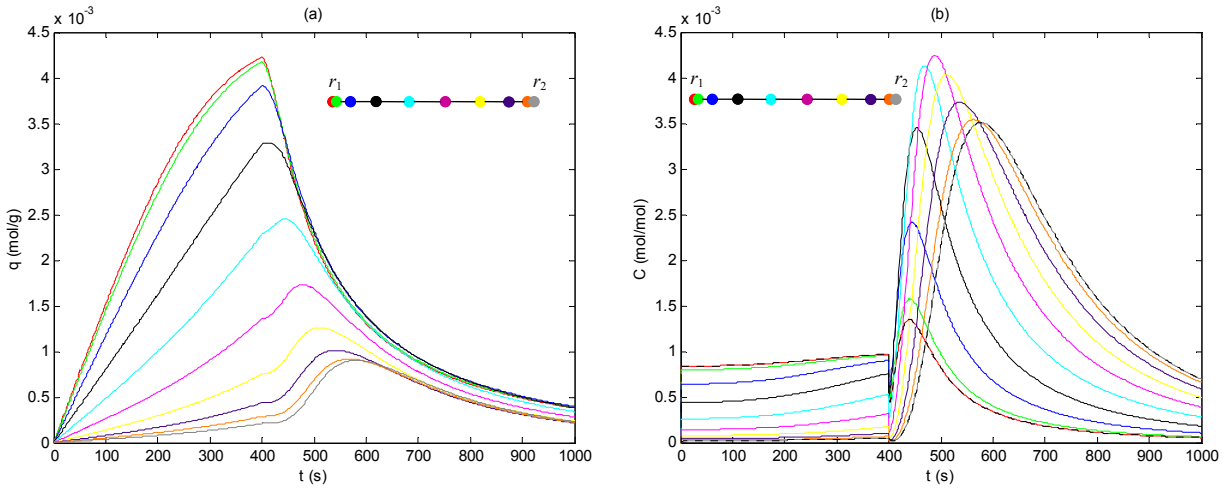

Figure 17 Simulation of consecutive adsorption-desorption - time profiles of the concentrations in 10 collocation points in the ads. bed (colored lines) and in the inlet and outlet tubes (---), for G_{ADS}=0.1 mol/s, G_{ED}=0.03 mol/s and U=10 V:
a) solid phase; b) gas phase

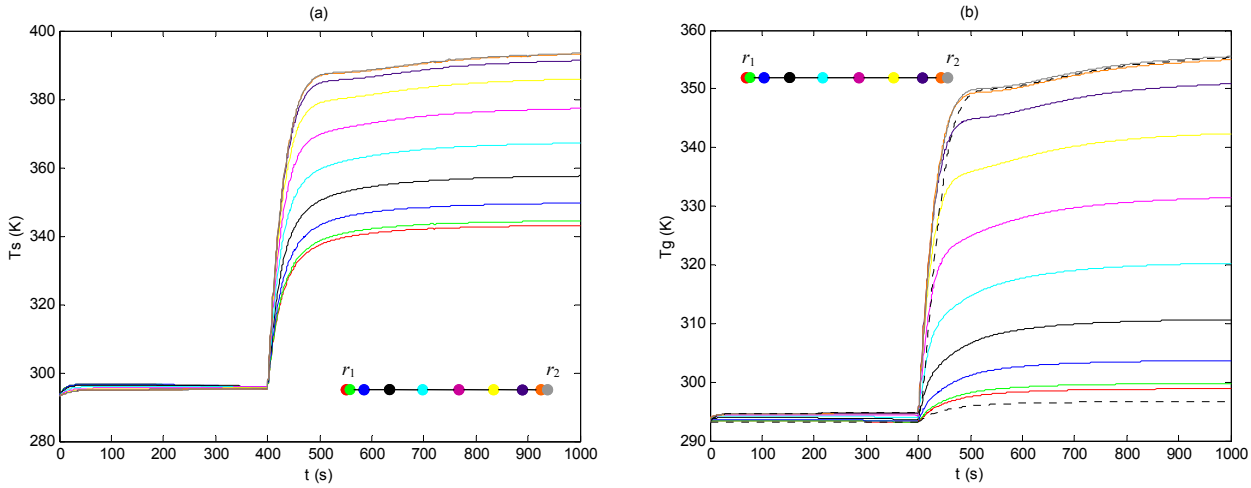

Figure 18 Simulation of consecutive adsorption-desorption - time profiles of the temperatures in 10 collocation points in the ads. bed (colored lines) and in the inlet and outlet tubes (---), for G_{ADS}=0.1 mol/s, G_{ED}=0.03 mol/s and U=10 V:
a) solid phase; b) gas phase

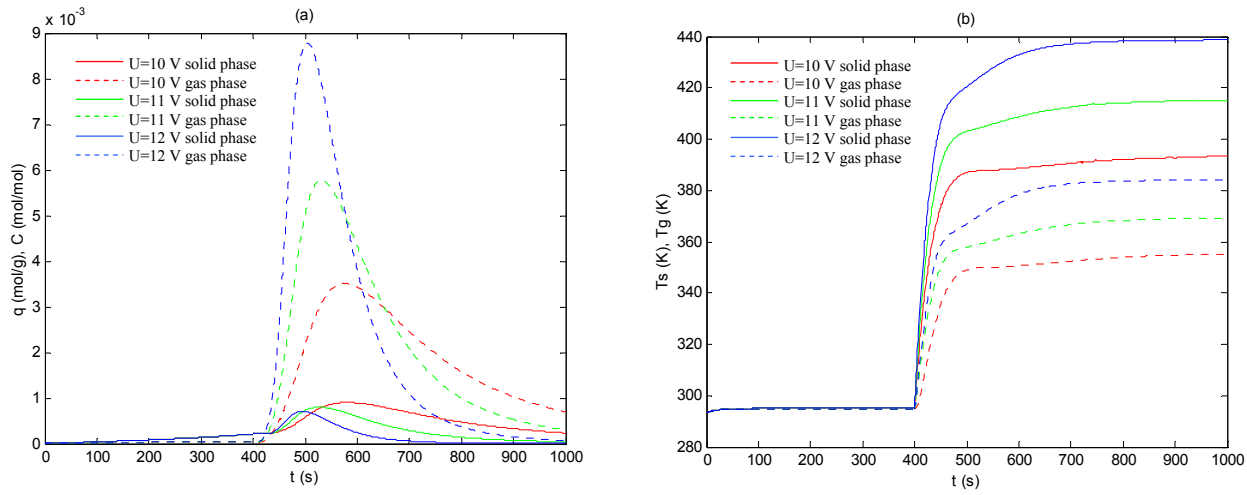

Figure 19 Simulation of consecutive adsorption-desorption – influence of electric voltage on the concentrations and temperatures at $r=r_2$ (solid) and in the outlet tube (gas) for G_{ADS}=0.1 mol/s and G_{ED}=0.03 mol/s:
a) concentrations i b) temperatures

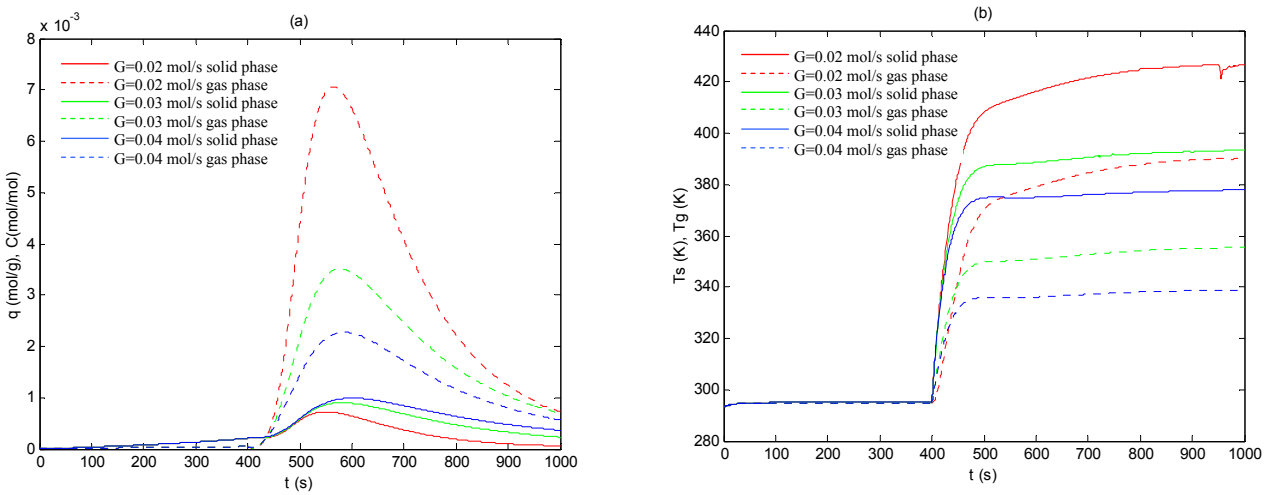

Figure 20 Simulation of consecutive adsorption-desorption – influence of the flow-rate during desorption on the concentrations and temperatures at $r=r_2$ (solid) and in the outlet tube (gas) for G_{ADS}=0.1 mol/s and U=10 V
a) concentrations i b) temperatures

3.7. Modeling and simulation of adsorption with reversed flow

In Section 3.1 the model was postulated for the annular cartridge-type adsorption bed with radial flow from the central pipe towards the outer surface of the cartridge, as shown in Figure 3. Nevertheless, in the system shown in Figure 1, during adsorption in some of the cartridges, the gas flow was in the reverse direction, i.e. from the periphery of the cartridge towards its central pipe (the upper cartridge in Figure 2) [3]. For a single cartridge configuration considered in this report, in this case the gas is introduced through the outer annular tube and it leaves the system through the central tube.

The model equations and some simulation results corresponding to this case are given in this section. The schematic representation of a differential volume element of the cartridge, used for setting up the model equations, is given in Figure 21. The assumptions listed at the beginning of Sections 3 are valid for this case as well.

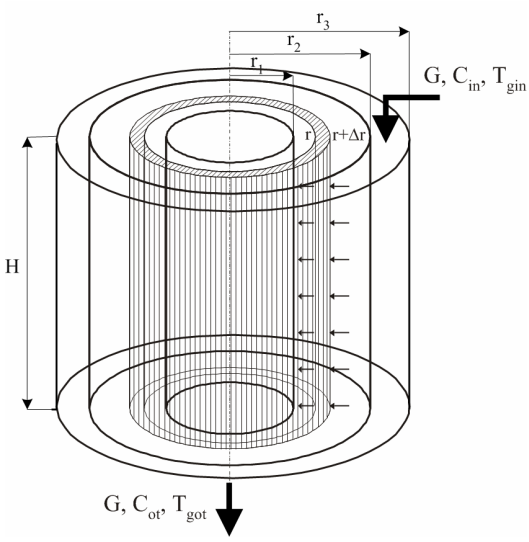

Figure 21 A differential volume element, used for modeling of adsorption with reversed flow

Model equations:

Compared to the model given in Section 3.1, the only differences are in the model equations for the central and the outer annular tube, and in the sign of the flow-terms in the material and energy balances for the gas phase in the adsorbent bed. Consecutively, the model is obtained as the following set of PDEs and ODEs:

Material balance for the solid phase within the adsorption bed: same as in Section 3.1 – equation (1)

Material balance for the gas phase within the adsorbent bed:

$$\rho_g \frac{\partial C}{\partial t} - \frac{G}{(2r\pi H\varepsilon_b)}\frac{\partial C}{\partial r} + (k_m a)(C - C^*) = \frac{D_m}{r}\frac{\partial}{\partial r}\left(r\frac{\partial C}{\partial r}\right) \tag{46}$$

Heat balance for the solid phase within the adsorption bed: same as in Section 3.1 – equation (3)

Heat balance for the gas phase within the adsorbent bed:

$$\rho_g(c_{pg} + c_{pv}C)\frac{\partial T_g}{\partial t} + \rho_g c_{pv}T_g\frac{\partial C}{\partial t} = \frac{G(c_{pg} + c_{pv}C)}{2r\pi H\varepsilon_b}\frac{\partial T_g}{\partial r} + \frac{Gc_{pv}T_g}{2r\pi H\varepsilon_b}\frac{\partial C}{\partial r} + (ha)(T_s - T_g) + \frac{D_t^{hg}}{r}\frac{\partial}{\partial r}\left(r\frac{\partial T_g}{\partial r}\right) \tag{47}$$

Material balance for the gas phase in the inlet annular tube:

$$(r_3^2 - r_2^2)\pi H\rho_g\frac{dC_{it}}{dt} = GC_{in} - GC_{it} + k_{m2}(2r_2\pi H)(1-\varepsilon_b)(C^*\big|_{r=r_2} - C_{it}) + 2r_2\pi H\varepsilon_b(C\big|_{r=r_2} - C_{it}) \tag{48}$$

Heat balance for the gas phase in the inlet annular tube:

$$(r_3^2 - r_2^2)\pi H \rho_g \frac{d}{dt}\left[(c_{pg} + c_{pv}C_{it})T_{git}\right] = G(c_{pg} + c_{pv}C_{in})T_{gin} - G(c_{pg} + c_{pv}C_{it})T_{git} + h_{s2}(2r_2\pi H)(1-\varepsilon_b)(T_{s|r=r_2} - T_{git}) + h_{g2}(2r_2\pi H\varepsilon_b)(T_{g|r=r_2} - T_{git}) - h_{wg}(2r_3\pi H)(T_{git} - T_a) \quad (49)$$

Material balance for the gas phase in the outlet central tube:

$$r_1^2\pi H\rho_g \frac{dC_{ot}}{dt} = G\,C\big|_{r=r_1} - GC_{ot} + k_{m1}(2r_1\pi H)(1-\varepsilon_b)(C^*\big|_{r=r_1} - C_{ot}) + 2r_1\pi H\varepsilon_b(C\big|_{r=r_1} - C_{ot}) \quad (50)$$

Heat balance for the gas phase in the outlet central tube:

$$r_1^2\pi H\rho_g \frac{d}{dt}\left[(c_{pg} + c_{pv}C_{ot})T_{got}\right] = G(c_{pg} + c_{pv}\,C\big|_{r=r_1})T_{g|r=r_1} - G(c_{pg} + c_{pv}C_{ot})T_{got} + h_{s1}(2r_1\pi H)(1-\varepsilon_b)(T_{s|r=r_1} - T_{got}) + h_{g1}(2r_1\pi H\varepsilon_b)(T_{g|r=r_1} - T_{got}) \quad (51)$$

Initial conditions – same as in Section 3.1 – equation (11):

Boundary conditions:

$$r=r_1:\quad D_t^{hs}\frac{\partial T_s}{\partial r}\bigg|_{r=r_1} = h_{s1}(T_s - T_{got})\ ,\quad D_t^{hg}\frac{\partial T_g}{\partial r}\bigg|_{r=r_1} = h_{g1}(T_g - T_{got})\ ,\ D_m\frac{\partial C}{\partial r}\bigg|_{r=r_1} = C - C_{ot} \quad (52)$$

$$r=r_2:\quad -D_t^{hs}\frac{\partial T_s}{\partial r}\bigg|_{r=r_2} = h_{s2}(T_s - T_{git})\ ,\quad -D_t^{hg}\frac{\partial T_g}{\partial r}\bigg|_{r=r_2} = h_{g2}(T_g - T_{git})\ ,-D_m\frac{\partial C}{\partial r}\bigg|_{r=r_1} = C - C_{it} \quad (53)$$

These model equations were solved in an analogous way as the ones defined in Section 3.1, i.e., by transforming the PDEs into approximate sets of ODEs, using the method of orthogonal collocations, and solving the resulting set of nonlinear 2*N*+6 ODEs (*N* being the number of internal collocation points), numerically.

The model presented in this section was used for simulation of adsorption with flow from the periphery towards the center of the cartridge. A sample of the simulated time profiles of the solid and gas concentrations in 10 collocation points and in the inlet and outlet tubes is presented in Figure 22, and the corresponding temperatures in Figure 23. Most of the model parameters were the same as in Section 3.4 (listed in Table 1), nevertheless, some of the parameters had to be changed in order to avoid convergence problems. Instead the values given in Table 1, the following values were used: k_{m1}=k_{m2}=3×10^{-7} mol/(cm^{2}s), h_{g2}=2×10^{-2} W/(cm^{2}K), D_t^{hs}=1.2×10^{-5} W/(cmK).

The simulated concentration and temperature profiles obtained for two different gas flow directions have similar shapes, i.e. no substantial difference of the two processes could be observed. A somewhat unusual shape of the curves corresponding to the collocation points close to the outer surface of the adsorption bed could be a result of numerical unstability, but it needs further analysis.

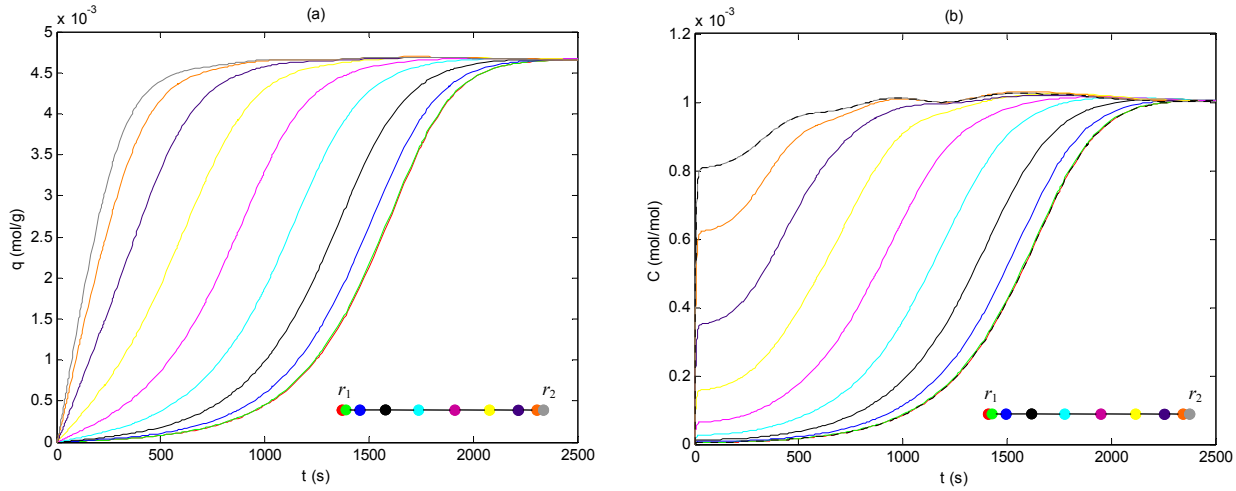

Figure 22 Simulation of adsorption with reversed flow- time profiles of the concentrations in 10 collocation points in the ads. bed (colored lines) and in the inlet and outlet tubes (---), for G=0.06 mol/s : a) solid phase; b) gas phase

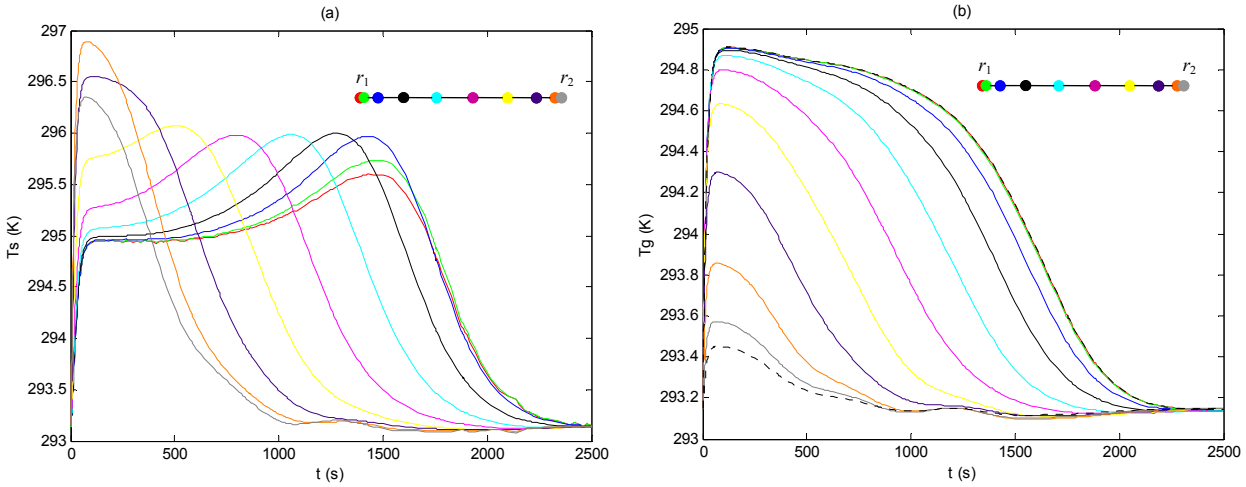

Figure 23 Simulation of adsorption with reversed flow- time profiles of the temperatures in 10 collocation points in the ads. bed (colored lines) and in the inlet and outlet tubes (---), for G=0.06 mol/s : a) solid phase; b) gas phase

4. Mathematical model of the single-cartridge adsorber with a layered (nonhomogeneous) adsorbent bed

The model presented in Section 3 was based on the assumption that the adsorbent bed can be treated as homogeneous. Nevertheless, in reality, the ACFC adsorbent bed under consideration is made of several layers of tissue made of activated carbon. Each layer, on the other hand, is a complex weaved structure made of yarns, each of them consisting of a great number of fine carbon fibers. The model presented in this section takes into account the existence of separate layers of carbon tissue in the bed, but neglects the finer structure, i.e., it assumes that each layer itself is a homogeneous, porous structure.

A simple analysis, based on ACFC density experimental data, justifies using such a model. E.g., for American Kynol ACFC-5092-20 adsorbent, the porosity of the material itself (single layer) is 0.513 [10], which is considerably lower than the average porosity of the whole adsorption bed which is ~0.72 [3]. Based on these values and the data about the thickness of a single ACFC layer Δ_I=0.55 mm [10], it was possible to calculate the gap between two layers: Δ_{II}=0.157 mm.

A schematic representation of the layered ACFC radial-flow adsorption bed is shown in Figure 24. Only the model for gas inlet through the central tube will be considered. The model for the reversed flow can be obtained in an analogous way as described in Section 3.7.

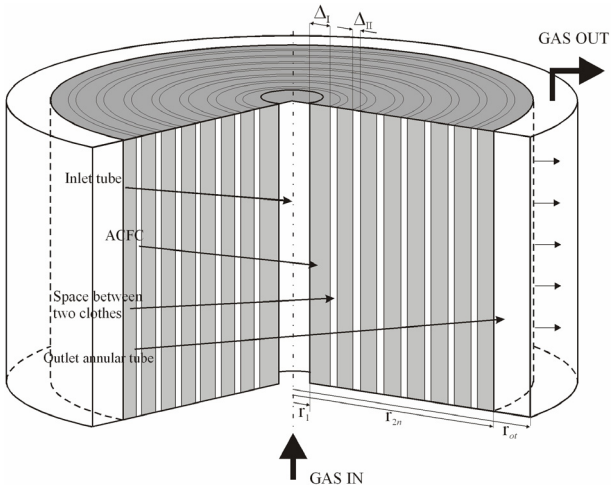

Slika 24 A schematic representation of the annular - radial flow - adsorbent bed made of layers of ACFC

In postulating this model, two zones of the adsorption bed were considered: ZONE I – consisting of the carbon tissue layers, and ZONE II – consisting of the gaps between the layers. Each zone consists of a number of sections, (sections of ZONE I and ZONE II interchanging regularly).

For an adsorption bed made of n layers of tissue, the mathematical model consists of the material and energy balances for the solid and for the gas phase within the ACFC layer, the material and energy balances for the gas phase in the gaps between the layers and the material and energy balances for the gas phase in the inlet and in the outlet tube. The assumptions listed in Section 3 were used for postulating of this model as well. In addition, it was assumed that the gas in the space between two layers is practically mixed.

4.1. Model equations

For these assumptions, the mathematical model of an adsorption bed made of n layers consists of $4n$ PDEs (mass and heat balances for ZONE I) and $2n$+2 ODEs (mass and heat balances for ZONE II and the inlet and outlet tube).

For sections of ZONE I - ACFC layers

Adsorbate balance for the solid phase:

$$\rho_c \frac{\partial q_k}{\partial t} = (k_m a)(C_k - C_k^*), \quad k=1,3,5,...,2n\text{-}1 \tag{54}$$

Adsorbate balance for the gas phase:

$$\rho_g \frac{\partial C_k}{\partial t} + \frac{G}{2r\pi H\varepsilon_c}\frac{\partial C_k}{\partial r} + (k_m a)(C_k - C_k^*) = \frac{D_m}{r}\frac{\partial}{\partial r}\left(r\frac{\partial C_k}{\partial r}\right), \quad k=1,3,5,...,2n\text{-}1 \tag{55}$$

Heat balance for the solid phase:

$$\rho_c(c_{ps} + c_{pl}q_k)\frac{\partial T_{sk}}{\partial t} + \rho_c c_{pl} T_{sk}\frac{\partial q_k}{\partial t} = \frac{\delta Q_{el}}{dV} + \Delta H_{ads}\rho_c\frac{\partial q_k}{\partial t} + \frac{D_t^{hs}}{r}\frac{\partial}{\partial r}\left(r\frac{\partial T_{sk}}{\partial r}\right) - (ha)(T_{sk} - T_{gk}) \tag{56}$$

k=1,3,5,...,2n-1

Heat balance for the gas phase:

$$\rho_g(c_{pg} + c_{pv}C_k)\frac{\partial T_{gk}}{\partial t} + \rho_g c_{pv} T_{gk}\frac{\partial C_k}{\partial t} = -\frac{G(c_{pg} + c_{pv}C_k)}{2r\pi H\varepsilon_c}\frac{\partial T_{gk}}{\partial r} - \frac{Gc_{pv}T_{gk}}{2r\pi H\varepsilon_c}\frac{\partial C_k}{\partial r} + (ha)(T_{sk} - T_{gk}) + \frac{D_t^{hg}}{r}\frac{\partial}{\partial r}\left(r\frac{\partial T_{gk}}{\partial r}\right) \tag{57}$$

k=1,3,5,...,2n-1

For sections of ZONE II - Gaps between two layers

Adsorbate balance:

$$\begin{aligned}(r_{k+1}^2 - r_k^2)\pi H\rho_g\frac{dC_k}{dt} = {} & G\,C_{k-1}\big|_{r=r_k} - GC_k + k_{mk}(2r_k\pi H)(1-\varepsilon_c)(C_{k-1}^*\big|_{r=r_k} - C_k) + \\ & k_{mk+1}(2r_{k+1}\pi H)(1-\varepsilon_c)(C_{k+1}^*\big|_{r=r_{k+1}} - C_k) + \\ & 2r_k\pi H\varepsilon_c(C_{k-1}\big|_{r=r_k} - C_k) + 2r_{k+1}\pi H\varepsilon_c(C_{k+1}\big|_{r=r_{k+1}} - C_k)\end{aligned}, \quad k=2,4,6,...2n\text{-}2 \tag{58}$$

Heat balance:

$$\begin{aligned}(r_{k+1}^2 - r_k^2)\pi H\rho_g\frac{d}{dt}\left[(c_{pg} + c_{pv}C_k)T_{gk}\right] = {} & G(c_{pg} + c_{pv}C_{k-1}\big|_{r=r_k})T_{gk-1|r=r_k} - G(c_{pg} + c_{pv}C_k)T_{gk} \\ & + h_{sk}(2r_k\pi H)(1-\varepsilon_c)(T_{sk-1|r=r_k} - T_{gk}) + h_{gk}(2r_k\pi H\varepsilon_c)(T_{gk-1|r=r_k} - T_{gk}) + \\ & h_{sk+1}(2r_{k+1}\pi H)(1-\varepsilon_c)(T_{sk+1|r=r_{k+1}} - T_{gk}) + h_{gk+1}(2r_{k+1}\pi H\varepsilon_c)(T_{gk+1|r=r_{k+1}} - T_{gk})\end{aligned}, \tag{59}$$

k=2,4,6,...,2n-2

For the inlet and outlet tubes:

Adsorbate balance for the gas phase in the central inlet tube:

$$r_1^2\pi H\rho_g\frac{dC_{it}}{dt}=GC_{in}-GC_{it}+k_{m1}(2r_1\pi H)(1-\varepsilon_c)(C_1^*\big|_{r=r_1}-C_{it})+2r_1\pi H\varepsilon_c(C_1\big|_{r=r_1}-C_{it}) \tag{60}$$

Heat balance for the gas phase in the central inlet tube:

$$\begin{aligned}r_1^2\pi H\rho_g\frac{d}{dt}\Big[(c_{pg}+c_{pv}C_{it})T_{git}\Big]&=G(c_{pg}+c_{pv}C_{in})T_{gin}-G(c_{pg}+c_{pv}C_{it})T_{git}\\&+h_{s1}(2r_1\pi H)(1-\varepsilon_c)(T_{s1|r=r_1}-T_{git})+h_{g1}(2r_1\pi H\varepsilon_c)(T_{g1|r=r_1}-T_{git})\end{aligned} \tag{61}$$

Adsorbate balance for the gas phase in the outlet annular tube:

$$\begin{aligned}(r_{ot}^2-r_{2n}^2)\pi H\rho_g\frac{dC_{ot}}{dt}&=GC_{2n-1}\big|_{r=r_{16}}-GC_{ot}+k_{m2n}(2r_{2n}\pi H)(1-\varepsilon_c)(C_{2n-1}^*\big|_{r=r_{2n}}-C_{ot})+\\&2r_{2n}\pi H\varepsilon_c(C_{2n-1}\big|_{r=r_{2n}}-C_{ot})\end{aligned} \tag{62}$$

Heat balance for the gas phase in the outlet annular tube:

$$\begin{aligned}&(r_{ot}^2-r_{2n}^2)\pi H\rho_g\frac{d}{dt}\Big[(c_{pg}+c_{pv}C_{ot})T_{got}\Big]=G(c_{pg}+c_{pv}C_{2n-1}\big|_{r=r_{2n}})T_{g2n-1|r=r_{2n}}-G(c_{pg}+c_{pv}C_{ot})T_{got}\\&+h_{s2n}(2r_{2n}\pi H)(1-\varepsilon_c)(T_{s2n-1|r=r_{2n}}-T_{got})+h_{g2n}(2r_{2n}\pi H\varepsilon_c)(T_{g2n-1|r=r_{2n}}-T_{got})-h_{wg}(2r_{ot}\pi H)(T_{got}-T_a)\end{aligned} \tag{63}$$

In equations (54-59) the subscript k associated to the concentrations and temperatures denotes the section in the adsorbent bed, starting from its inner surface. The odd subscripts correspond to the sections of ZONE I, while the even ones correspond to the sections of ZONE II. The subscripts associated to the radial coordinate r correspond to the inner and outer diameters of the sections: e.g. the section k is bounded by r_k and r_{k+1}, r_1 is the diameter of the central inlet tube and r_{2n+1} of the outlet tube.

Initial and boundary conditions:

Initial conditions:

$$t<0,\ r\in[r_1,r_{2n}]:\quad T_g=T_s=T_{git}=T_{got}=T_{gin}=T_{go}=T_a=T_p,\qquad C=C_{it}=C_{ot}=C_{in}=C^*=\Phi(q)=C_p \tag{64}$$

Boundary conditions:

$$r=r_1:\ D_m\frac{\partial C_1}{\partial r}\bigg|_{r=r_1}=C_1-C_{it},\quad D_t^{hg}\frac{\partial T_{g1}}{\partial r}\bigg|_{r=r_1}=h_{g1}(T_{g1}-T_{git}),\ D_t^{hs}\frac{\partial T_{s1}}{\partial r}\bigg|_{r=r_1}=h_{s1}(T_{s1}-T_{got}) \tag{65}$$

$r=r_{k+1}$, for k=1,3,5,...,2n-3:

$$-D_m\frac{\partial C_k}{\partial r}\bigg|_{r=r_{k+1}}=C_k-C_{k+1},\ -D_t^{hg}\frac{\partial T_{gk}}{\partial r}\bigg|_{r=r_{k+1}}=h_{gk+1}(T_{gk}-T_{gk+1}),\ -D_t^{hs}\frac{\partial T_{sk}}{\partial r}\bigg|_{r=r_{k+1}}=h_{sk+1}(T_{sk}-T_{gk+1}) \tag{66}$$

$r=r_k$, k=3,5,...,$2n$-1:

$$D_m \left.\frac{\partial C_k}{\partial r}\right|_{r=r_k} = C_k - C_{k-1} \quad D_t^{hg} \left.\frac{\partial T_{gk}}{\partial r}\right|_{r=r_k} = h_{gk}(T_{gk} - T_{gk-1}), \quad D_t^{hs} \left.\frac{\partial T_{sk}}{\partial r}\right|_{r=r_k} = h_{sk}(T_{sk} - T_{gk-1}) \qquad (67)$$

$$r=r_{2n}: \; -D_m \left.\frac{\partial C_{2n-1}}{\partial r}\right|_{r=r_{2n}} = C_{2n-1} - C_{ot}, \; -D_t^{hg} \left.\frac{\partial T_{g2n-1}}{\partial r}\right|_{r=r_{2n}} = h_{g2n}(T_{g2n-1} - T_{got}), -D_t^{hs} \left.\frac{\partial T_{s2n-1}}{\partial r}\right|_{r=r_{2n}} = h_{s2n}(T_{s2n-1} - T_{got}) \qquad (68)$$

4.2. Numerical solution of the model equations

The model equations presented in this section were again solved numerically. The first step of the numerical solution was approximation of the PDEs, using the method of orthogonal collocation. This method was applied to each section of ZONE I. For convenience, the radial coordinate was again transformed into nondimensional form. For the k-th section, the nondimensional radial coordinate was defined in the following way:

$$u_k = \frac{r - r_k}{r_{k+1} - r_k} \qquad (69)$$

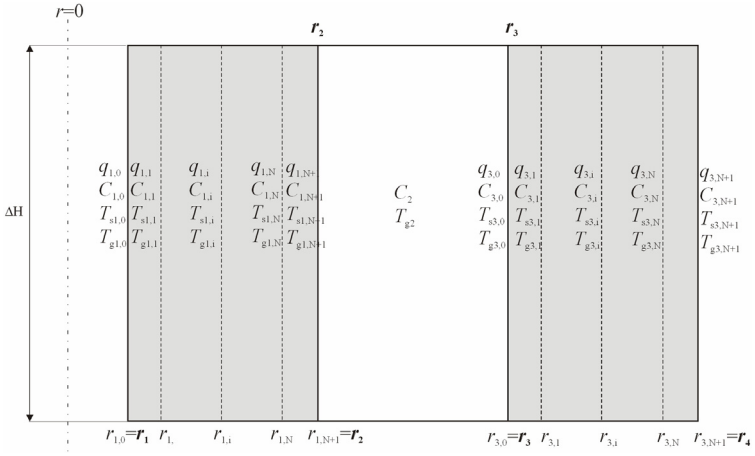

Figure 25 A schematic representation of the distribution of the collocation points in the first 3 sections

For each section of ZONE I, N internal collocation points were used, plus 2 points at the section boundaries. (In general the number of collocation points for different sections could be different, but in the analysis presented here, the same number was used for all sections.)

As an illustration, a schematic picture of the distribution of the collocation points and definition of the variables in the first 3 sections (the first two layers of tissue and the gap between them) is given in Figure 25.

Application of the orthogonal collocation method on PDEs (54-57) leads to the following set of ODEs:

$$\frac{dq_{k,i}}{dt} = \frac{k_m a}{\rho_b}(C_{k,i} - C^*_{k,i}), \quad i=0,...N+1, \quad k=1,3,5,\ldots,2n\text{-}1 \qquad (70)$$

$$\frac{dC_{k,i}}{dt} = -\frac{G\sum_{j=0}^{N+1} A_{k,i,j} C_{k,j}}{2\pi H \varepsilon_c \Delta_1 \rho_g (u_{k,i}\Delta_1 + r_k)} - \frac{k_m a}{\rho_g}(C_{k,i} - C^*_{k,i}) + \frac{D_m \sum_{j=0}^{N+1} B_{k,i,j} C_{k,j}}{(\Delta_1 u_{k,i} + r_k)\rho_g} \qquad (71)$$

i=1,….,N, k=1,3,5,…,$2n$-1

$$\frac{dT_{sk,i}}{dt}=\frac{U^2}{\rho_b(c_{ps}+c_{pl}q_{k,i})\rho_0(1+b(T_{sk,i}-T_R))H^2}+\frac{\Delta H_{ads}}{(c_{ps}+c_{pl}q_{k,i})}\frac{dq_{k,i}}{dt}+$$
$$+\frac{D_t^{hs}\sum_{j=0}^{N+1}B_{k,i,j,}T_{sk,j}}{\rho_b(c_{ps}+c_{pl}q_{k,i})(u_{k,i}\Delta_I+r_k)}-\frac{(ha)(T_{sk,i}-T_{gk,i})}{\rho_b(c_{ps}+c_{pl}q_{k,i})}-\frac{c_{pl}T_{sk,i}}{(c_{ps}+c_{pl}q_{k,i})}\frac{dq_{k,i}}{dt}, \quad (72)$$

i=1,…,N, k=1,3,5,…,2n-1

$$\frac{dT_{gk,i}}{dt}=-\frac{G\sum_{j=0}^{N+1}A_{k,i,j}T_{gk,j}}{2\rho_g(u_{k,i}\Delta_I+r_k)\pi H\varepsilon_c\Delta_I}-\frac{Gc_{pv}T_{gk,i}\sum_{j=0}^{N+1}A_{k,i,j}C_{k,j}}{\rho_g(c_{pg}+c_{pv}C_{k,i})2\pi H\varepsilon_c\Delta_I}+$$
$$\frac{ha(T_{sk,i}-T_{gk,i})}{\rho_g(c_{pg}+c_{pv}C_{k,i})}+\frac{D_t^{hg}\sum_{j=0}^{N+1}B_{k,i,j}T_{gk,j}}{(u_{k,i}\Delta_I+r_k)\rho_g(c_{pg}-c_{pv}C_{k,i})}-\frac{c_{pv}T_{gk,i}}{c_{pg}+c_{pv}C_{k,i}}\frac{dC_{k,i}}{dt}, \quad (73)$$

i=1,…,N, k=1,3,5,…,2n-1

In equations (70-73) the concentrations and temperatures are defined by two subscripts: the first one corresponds to the section and the second one to the collocation point of that section.

The equations corresponding to the sections of ZONE II and the inlet and outlet tubes have also be rewritten:

$$\frac{dC_k}{dt}=\frac{GC_{k-1,N+1}-GC_k}{(r_{k+1}^2-r_k^2)\pi H\rho_g}+\frac{k_{mk}(2r_k)(1-\varepsilon_c)(C^*_{k-1,N+1}-C_k)}{(r_{k+1}^2-r_k^2)\rho_g}+$$
$$\frac{k_{mk+1}(2r_{k+1})(1-\varepsilon_c)(C^*_{k+1,0}-C_k)}{(r_{k+1}^2-r_k^2)\rho_g}+\frac{2r_k\varepsilon_c(C_{k-1,N+1}-C_k)}{(r_{k+1}^2-r_k^2)\rho_g}+\frac{2r_{k+1}\varepsilon_c(C_{k+1,0}-C_k)}{(r_{k+1}^2-r_k^2)\rho_g} \quad (74)$$

k=2,4,…,2n-2

$$\frac{dT_{gk}}{dt}=\frac{G(c_{pg}+c_{pv}C_{k-1,N+1})T_{gk-1,N+1}}{(r_{k+1}^2-r_k^2)\pi H\rho_g(c_{pg}+c_{pv}C_k)}-\frac{GT_{gk}}{(r_{k+1}^2-r_k^2)\pi H\rho_g}+\frac{h_{sk}(2r_k)(1-\varepsilon_c)(T_{sk-1,N+1}-T_{gk})}{(r_{k+1}^2-r_k^2)\rho_g(c_{pg}+c_{pv}C_k)}+$$
$$\frac{h_{gk}(2r_k\varepsilon_c)(T_{gk-1,N+1}-T_{gk})}{(r_{k+1}^2-r_k^2)\rho_g(c_{pg}+c_{pv}C_k)}+\frac{h_{sk+1}(2r_{k+1})(1-\varepsilon_c)(T_{sk+1,0}-T_{gk})}{(r_{k+1}^2-r_k^2)\rho_g(c_{pg}+c_{pv}C_k)}+\frac{h_{gk+1}(2r_{k+1}\varepsilon_c)(T_{gk+1,0}-T_{gk})}{(r_{k+1}^2-r_k^2)\rho_g(c_{pg}+c_{pv}C_k)}- \quad (75)$$
$$\frac{c_{pv}T_{gk}}{(c_{pg}+c_{pv}C_k)}\frac{dC_k}{dt}$$

k=2,4,…,2n-2

$$\frac{dC_{it}}{dt}=\frac{G(C_{in}-C_{it})}{r_1^2\pi H\rho_g}+\frac{k_{m1}(2r_1\pi H)(1-\varepsilon_c)(C^*_{1,0}-C_{it})}{r_1^2\pi H\rho_g}+\frac{2r_1\pi H\varepsilon_c(C_{1,0}-C_{it})}{r_1^2\pi H\rho_g} \quad (76)$$

$$\frac{dT_{git}}{dt}=\frac{G(c_{pg}+c_{pv}C_{in})T_{gin}}{r_1^2\pi H\rho_g(c_{pg}+c_{pv}C_{it})}-\frac{GT_{git}}{r_1^2\pi H\rho_g}+\frac{h_{s1}(2r_1\pi H)(1-\varepsilon_c)(T_{s1,0}-T_{git})}{r_1^2\pi H\rho_g(c_{pg}+c_{pv}C_{it})}+$$
$$\frac{h_{g1}(2r_1\pi H\varepsilon_c)(T_{g1,0}-T_{git})}{r_1^2\pi H\rho_g(c_{pg}+c_{pv}C_{it})}-\frac{c_{pv}T_{git}}{(c_{pg}+c_{pv}C_{it})}\frac{dC_{it}}{dt} \quad (77)$$

$$\frac{dC_{ot}}{dt}=\frac{G(C_{2n-1,N+1}-C_{ot})}{(r_{ot}^2-r_{2n}^2)\pi H\rho_g}+\frac{k_{m2n}(2r_{2n}\pi H)(1-\varepsilon_c)(C^*_{2n-1,N+1}-C_{ot})}{(r_{ot}^2-r_{2n}^2)\pi H\rho_g}+\frac{2r_{2n}\pi H\varepsilon_c(C_{2n-1,N+1}-C_{ot})}{(r_{ot}^2-r_{2n}^2)\pi H\rho_g} \quad (78)$$

$$\frac{dT_{got}}{dt}=\frac{G(c_{pg}+c_{pv}C_{2n-1,N+1})T_{g2n-1,N+1}}{(r_{ot}^2-r_{2n}^2)\pi H\rho_g(c_{pg}+c_{pv}C_{ot})}-\frac{GT_{got}}{(r_{ot}^2-r_{2n}^2)\pi H\rho_g}+\frac{h_{s2n}(2r_{2n}\pi H)(1-\varepsilon_c)(T_{s2n-1,N+1}-T_{got})}{(r_{ot}^2-r_{2n}^2)\pi H\rho_g(c_{pg}+c_{pv}C_{ot})}+$$
$$\frac{h_{g2n}(2r_{2n}\pi H\varepsilon_c)(T_{g2n-1,N+1}-T_{got})}{(r_{ot}^2-r_{2n}^2)\pi H\rho_g(c_{pg}+c_{pv}C_{ot})}-\frac{h_{wg}(2r_{ot}\pi H)(T_{got}-T_a)}{(r_{ot}^2-r_{2n}^2)\pi H\rho_g(c_{pg}+c_{pv}C_{ot})}-\frac{c_{pv}T_{got}}{(c_{pg}+c_{pv}C_{ot})}\frac{dC_{ot}}{dt} \quad (79)$$

After applying the method of orthogonal collocation, the boundary conditions were obtained in the algebraic form:

- For k=1: $C_{1,0}=\dfrac{C_{it}+D_m\dfrac{1}{\Delta_I}\sum_{j=1}^{N+1}A_{1,o,j}C_j}{1+D_m\dfrac{1}{\Delta_I}A_{1,0,0}}$,

$$T_{g1,0}=\frac{h_{g1}T_{git}+D_t^{hg}\dfrac{1}{\Delta_I}\sum_{j=1}^{N+1}A_{1,0,j}T_{g1,j}}{h_{g1}+D_t^{hg}\dfrac{1}{\Delta_I}A_{1,0,0}},\quad T_{s1,0}=\frac{h_{s1}T_{git}+D_t^{hs}\dfrac{1}{\Delta_I}\sum_{j=1}^{N+1}A_{1,0,j}T_{s1,j}}{h_{s1}+D_t^{hs}\dfrac{1}{\Delta_I}A_{1,0,0}} \quad (80)$$

- For k=3,5,...,2n-1: $C_{k,0}=\dfrac{C_{k-1,N+1}+D_m\dfrac{1}{\Delta_I}\sum_{j=1}^{N+1}A_{k,0,j}C_{k,j}}{1-D_m\dfrac{1}{\Delta_I}A_{k,0,0}}$,

$$T_{sk,0}=\frac{h_{sk}T_{gk-1,N+1}+D_t^{hs}\dfrac{1}{\Delta_I}\sum_{j=1}^{N+1}A_{k,0,j}T_{sk,j}}{h_{sk}-D_t^{hs}\dfrac{1}{\Delta_I}A_{k,0,0}},\quad T_{gk,0}=\frac{h_{gk}T_{gk-1,N+1}+D_t^{hg}\dfrac{1}{\Delta_I}\sum_{j=1}^{N+1}A_{k,0,j}T_{gk,j}}{h_{gk}-D_t^{hg}\dfrac{1}{\Delta_I}A_{k,0,0}} \quad (81)$$

- For k=1,3,...,2n-3: $C_{k,N+1} = \dfrac{C_{k+1,0} - D_m \dfrac{1}{\Delta_I} \sum_{j=0}^{N} A_{k,N+1,j} C_{k,j}}{1 + D_m \dfrac{1}{\Delta_I} A_{k,N+1,N+1}}$,

$$T_{sk,N+1} = \frac{h_{sk+1} T_{gk+1,0} - D_t^{hs} \dfrac{1}{\Delta_I} \sum_{j=0}^{N} A_{k,N+1,j} T_{sk,j}}{h_{sk+1} + D_t^{hs} \dfrac{1}{\Delta_I} A_{k,N+1,N+1}}, \quad T_{gk,N+1} = \frac{h_{gk+1} T_{gk+1,0} - D_t^{hg} \dfrac{1}{\Delta_I} \sum_{j=0}^{N} A_{k,N+1,j} T_{gk,j}}{h_{gk+1} + D_t^{hg} \dfrac{1}{\Delta_I} A_{k,N+1,N+1}} \tag{83}$$

- For k=2n-1: $C_{2n-1,N+1} = \dfrac{C_{ot} - D_m \dfrac{1}{\Delta_I} \sum_{j=0}^{N} A_{2n-1,N+1,j} C_{2n-1,j}}{1 + D_m \dfrac{1}{\Delta_I} A_{2n-1,N+1,N+1}}$,

$$T_{g2n-1,N+1} = \frac{h_{g2n} T_{got} - D_t^{hg} \dfrac{1}{\Delta_I} \sum_{j=0}^{N} A_{2n-1,N+1,j} T_{g2n-1,j}}{h_{g2n} + D_t^{hg} \dfrac{1}{\Delta_I} A_{2n-1,N+1,N+1}},$$

$$T_{s2n-1,N+1} = \frac{h_{s2n} T_{got} - D_t^{hs} \dfrac{1}{\Delta_I} \sum_{j=0}^{N} A_{2n-1,N+1,j} T_{s2n-1,j}}{h_{s2n} + D_t^{hs} \dfrac{1}{\Delta_I} A_{2n-1,N+1,N+1}} \tag{84}$$

with:

$$A_{k,i,j} = \left(\frac{dl_{k,j}}{du_k} \right)_{u_k = u_{k,i}}, \qquad B_{k,i,j} = \frac{u_{k,i} \Delta_I + r_k}{\Delta_I^2} \left(\frac{d^2 l_j}{du_k^2} \right)_{u_k = u_{k,i}} + \frac{1}{\Delta_I} \left(\frac{dl_{k,j}}{du_k} \right)_{u_k = u_{k,i}} \tag{85}$$

4.3. Simulation of adsorption and electrothermal desorption

The derived model was used for simulation of adsorption, electroresistive heating and electrothermal desorption. The simulation was performed for an adsorption bed made of 8 layers of ACFC. The same system was used as in Section 3. Owing to the model complexity and the large number of equations to be solved, the model was solved for 3 collocation points in each section of ZONE I (1 internal plus 2 border points). The model parameters that differ from those used in Section 3 are listed in Table 2. The rest have the values given in Table 1.

A small portion of the simulation results is given, as illustration.

Figures 26 and 27 show the simulation results for adsorption on an initially clean adsorption bed. The time profiles of the concentrations in the solid phase in different layers of the bed (sections of ZONE I) are presented in Fig. 26(a) (red, green and blue lines correspond to different collocation points), and the time profiles of the concentrations in the gas phase in both zones (red, green and blue lines correspond to different collocation points in the sections of ZONE I, while the dashed cyan lines correspond to the sections of ZONE II), as well as in the inlet and outlet tubes (dashed black lines), are given in Fig. 26(b). The corresponding

temperatures are shown in Figure 27 (the solid temperatures in Fig. 27(a) and the gas temperatures in Fig. 27(b)).

An interesting result of this simulation is that the lines corresponding to the concentrations of the gas phase at two neighbouring surfaces in two ACFC layers practically overlap, as well as the concentration of the gas between those two layers. A similar situation is with the concentrations in the solid phase. Nevertheless, the lines corresponding to the temperatures of two neighbouring surfaces are distinct.

Table 2. Additional model parameters used for simulation of adsorption, electroresistive heating and electrothermal desorption, using a model for a layered adsorption bed

Variable	Notation and value	
	Adsorption	Heating/Desorption
Outer diameter of the outlet annular tube	r_{ot}=3.55 cm	
Cloth thickness	Δ_I=0.055 cm	
Gap between two layers of ACFC	Δ_{II}=0.0157 cm	
Cloth porosity	ε_c=0.513	
Mass transfer coefficient	k_m=0.0004 mol/(cm^{2}s)	
Mass transfer coefficients from the solid in zone I to the gas phase in the inlet and outlet annular tube	$k_{m1}=k_{m16}=5\times10^{-5}$ mol/(cm^{2}s)	
Mass transfer coefficients from the solid in zone I to gas in zone II	$k_{m2}=k_{m3}=\ldots=k_{m15}=2\times10^{-1}$ mol/(cm^{2}s)	
Solid to gas heat transfer coefficient in zone I	$h=4\times10^{-4}$ W/(cm^{2}K)	$h=6\times10^{-4}$ W/(cm^{2}K)
Heat transfer coefficients from solid in zone I to gas in zone II	$h_{s2}=h_{53}=\ldots=h_{s15}=1\times10^{-5}$ W/(cm^{2}K)	
Heat transfer coefficients from solid to gas in the inlet tube	$h_{s1}=1.35\times10^{-5}$ W/(cm^{2}K)	
Heat transfer coefficients from solid to gas in the outlet annular tube	$h_{s16}=8.7\times10^{-6}$ W/(cm^{2}K)	
Heat transfer coefficient from gas in zone I to gas in the inlet tube	$h_{g1}=8\times10^{-5}$W/(cm^{2}K)	
Heat transfer coefficient from gas in zone I to gas in the outlet annular tube	$h_{g16}=2\times10^{-5}$W/(cm^{2}K)	
Heat transfer coefficient from gas in zone I to gas in zone II	$h_{g2}=h_{g3}=\ldots=h_{g15}=6\times10^{-5}$ W/(cm^{2}K)	
Heat diffusivity of the solid phase	$D_t^{hs}=5\times10^{-6}$ W/(cmK)	
Heat diffusivity of the gas phase in zone I	$D_t^{hg}=1\times10^{-6}$W/(cmK)	
Radial mass transfer dispersion coefficient	$D_m=9\times10^{-6}$ mol/(cms)	$D_m=5\times10^{-5}$ mol/(cms)
Adsorbent bed density	ρ_c=0.276 g/cm^3	

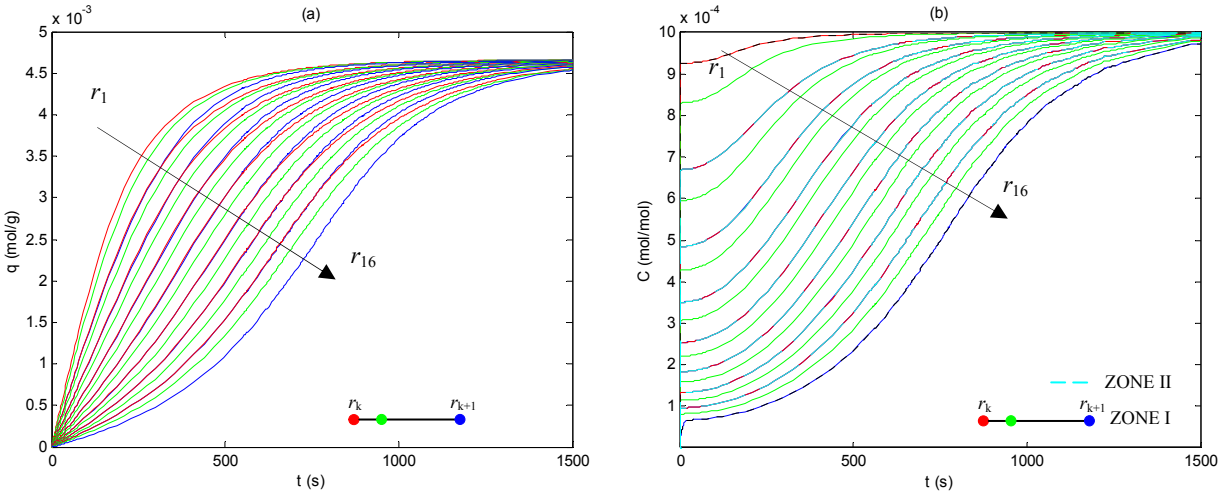

Figure 26 Simulation of adsorption for 8 layers of ACFC – time profiles of the concentrations in all sections of ZONE I and ZONE II and in the inlet and outlet tube (----), for G=0.1 mol/s: a) Solid phase; b) Gas phase

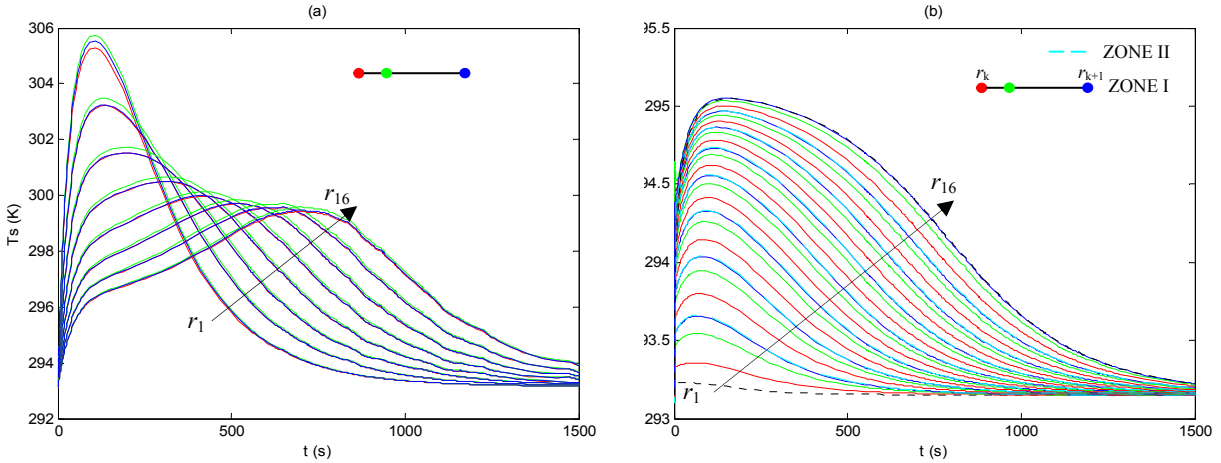

Figure 27 Simulation of adsorption for 8 layers of ACFC – time profiles of the temperatures in all sections of ZONE I and ZONE II and in the inlet and outlet tube (----), for G=0.1 mol/s: a) Solid phase; b) Gas phase

The simulated time profiles of the temperatures during electroresistive heating are shown in Figure 28. On the other hand, the simulation results of electrothermal desorption are presented in Figure 29 (the concentration profiles in different sections of ZONE I and ZONE II) and Figure 30 (the temperature profiles).

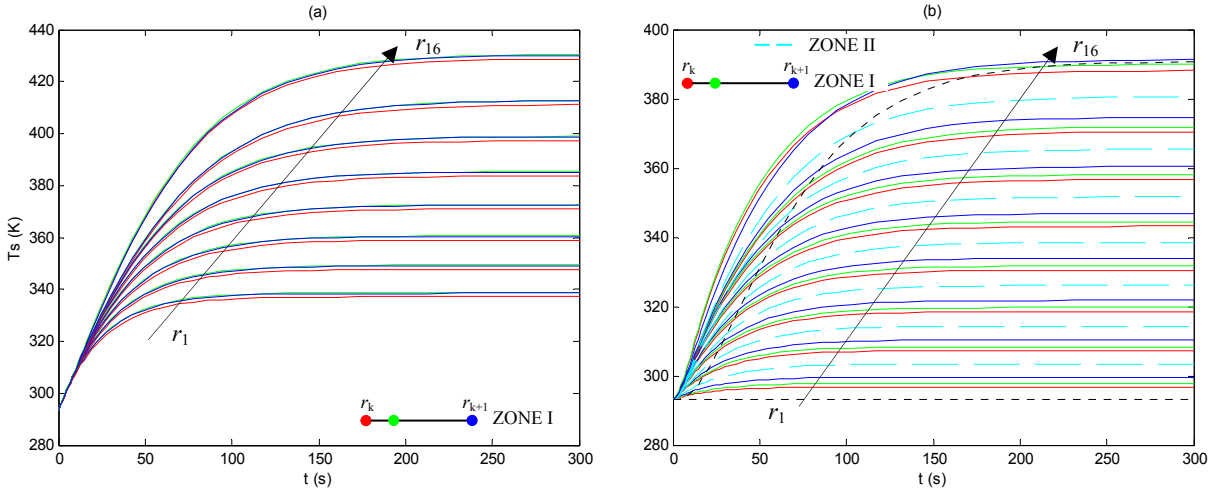

Figure 28 Simulation of electroresistive heating for 8 layers of ACFC – time profiles of the temperatures in all sections of ZONE I and ZONE II and in the inlet and outlet tube (----), for G=0.02 mol/s and U=8V: a) Solid phase; b) Gas phase

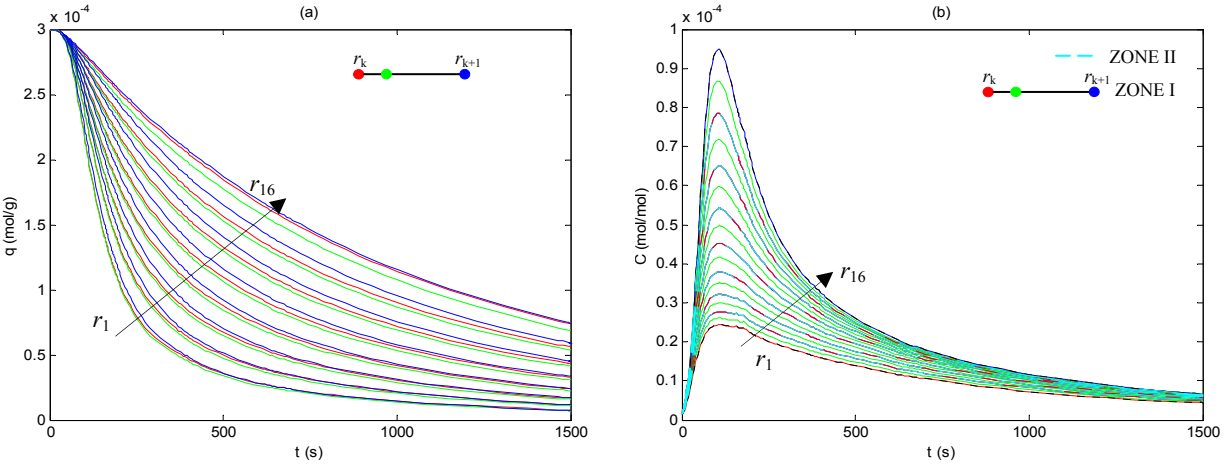

Figure 29 Simulation of electrothermal desorptions for 8 layers of ACFC – time profiles of the concentrations in all sections of ZONE I and ZONE II and in the inlet and outlet tube (----), for G=0.02 mol/s and U=8V: a) Solid phase; b) Gas phase

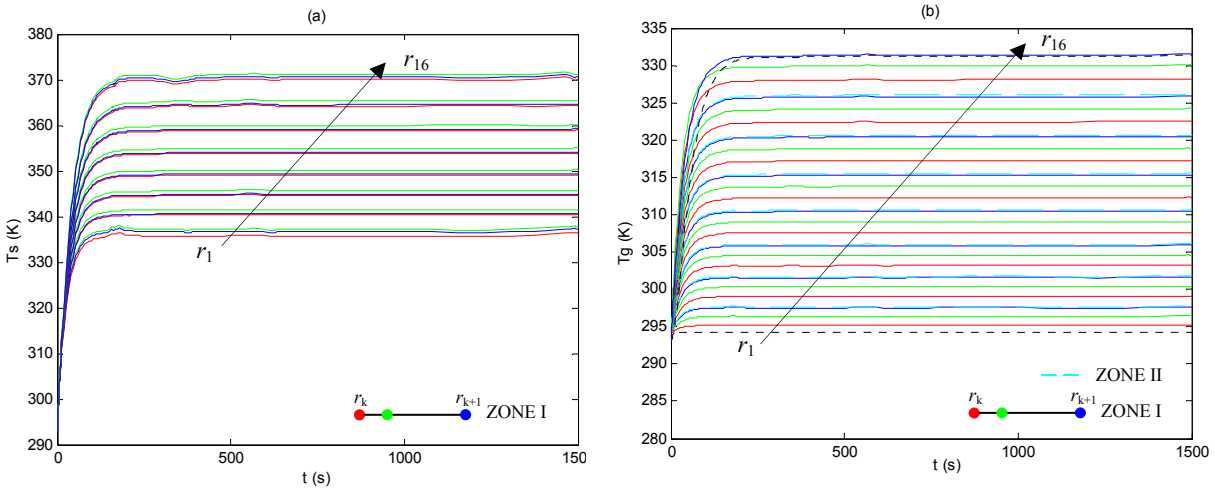

Figure 30 Simulation of electrothermal desorptions for 8 layers of ACFC – time profiles of the temperatures in all sections of ZONE I and ZONE II and in the inlet and outlet tube (----), for G=0.02 mol/s and U=8V: a) Solid phase; b) Gas phase

5. CONCLUSIONS

This report summarizes the results of mathematical modeling of the central unit of the TSA system with electrothermal desorption – the adsorption bed. The modeling was performed for an annular, radial-flow ACFC adsorber, used in Ref. [3]. Two models of different complexity were postulated and the procedures for their numerical solution were established. The models were used for simulation of adsorption, electroresistive heating and electrothermal desorption, as well as combined adsortion-desorption. The equilibrium, and part of the transport parameters in the model equations were calculated using correlations from literature. Nevertheless, some of the parameters had to be assumed, as correlations for their estimation are not available.

The idea of this modeling is to incorporate the derived models for the adsorber into a mathematical model, which would describe the whole TSA system. As the adsorber represents the main, and, from the modeling point of view, the most complex part of the system, the development of its models is crucial.

One of the important issues, that have to be resolved in the further work, is getting reliable correlations for calculation of the transport parameters in an adsorbent bed with fibrous structure, such as the one made of ACFC. To our knowledge, such correlations are not available in the literature. In order to define them, serious experimental investigation is needed. The other issue is the necessity for experimental verification of the models, which would enable their comparison and critical evaluation.

Nomenclature

a(m^2/m^3)	- Specific surface area
b(K^{-1})	- Temperature coefficient of the bed electrical resistivity
C(mol/mol)	- Adsorbate concentration in the gas phase
C^*(mol/mol)	- Adsorbate concentration in the gas phase in equilibrium with the solid phase
c_{pg}(J/mol/K)	- Specific heat capacity of the inert gas
c_{pl}(J/mol/K)	- Specific heat capacity of liquid adsorbate
c_{ps}(J/g/K)	- Heat capacity of the solid phase
c_{pv}(J/mol/K)	- Specific heat capacity of gaseous adsorbate
D_{AB}(mol/cm/s)	- Molecular diffusivity of the gas phase
D_m (mol/cm/s)	- Radial mass transfer dispersion coefficient
D_p(cm)	- Fiber diameter
D_t^{hg}(W/K/cm)	- Heat diffusivity of the gas phase
D_t^{hs}(W/K/cm)	- Heat diffusivity of the solid phase
E(J/mol)	- Adsorption energy of the adsorbate (D-R eq.)

g(cm/s^2) -Gravitation constant

G(mol/s) - Flow rate of the inert gas

H(cm) - Bed axial dimension

h(J/cm^2/K) - Solid to gas heat transfer coefficient

h_{wg}(J/cm^2/K) - Gas to ambient heat transfer coefficient (heat losses)

k(W/cm/K) - Gas phase thermal conductivity

k_b(J/K) - Boltzmann's constant

k_m(mol/cm^2/s) - Mass transfer coefficient

M_A(g/mol) - Adsorbate molar mass

M_B(g/mol) - Inert gas molar mass

N - Number of internal collocation points in the radial direction

Nu - Nusselt number

p(kPa) - Gas pressure

p_A - Adsorbate partial pressure

p_{cA}(kPa) - Critical pressure of the adsorbate

p_{cB}(kPa) - Critical pressure of the inert gas

p^o(kPa) - Adsorbate saturation vapor pressure

Pe - Peclet number

Pr - Prandtl number

q(mol/g) - Adsorbate concentration in the solid phase

Q_{el}(J/s) - Joule's heat

Ra - Rayleigh number

Re - Reynolds number

R_g(J/mol/K) - Gas constant

r_1(cm) - Inner diameter of the cartridge

r(cm) - Bed radial dimension

R_{el}(Ω) - Electric resistance

Sc - Schmidt number

Sh - Sherwood number

T_a(K) - Ambient temperature

T_{cA}(K) - Critical temperature of the adsorbate

T_{cB}(K) - Critical temperature of the inert gas

T_g(K) - Gas phase temperature

T_R(K) - Referent temperature

T_s(K) - Solid phase temperature

U(V) - Electric potential difference

u - Non-dimensional radial column coordinate

v - Superficial gas velocity

VP_A, VP_B, VP_C, VP_D - Wagner constants for the adsorbate

W(cm^3/g) - Adsorbate volume per 1g of the adsorbent mass

W_0(cm^3/g) - Total volume of micropores (D-R equation)

ΔH_{ads}(J/g) - Heat of adsorption

Greek letters:

α(cm^2/s) - Thermal diffusivity of the gas phase

β(1/K) - Reciprocal of the film temperature

Δ(cm) - Bed thickness

ε_b - Bed porosity

ε_c - Cloth porosity

μ (Pa/s) - Dynamic viscosity

ν(cm^2/s) - Kinematic viscosity of the gas phase

ρ(Ωcm) - Electric resistivity

ρ_0(Ωcm) - Electric resistivity at referent temperature T_R

ρ_b(g/cm^3) - Adsorbent bed density

ρ_g(mol/cm^3) - Density of the inert gas

ρ_A(g/cm^3) - Adsorbate density

Subscripts:

b - bed

c - cloth

g - gas

in - inlet

o - outlet

p - previous (initial)

s - solid phase

it - inlet tube

ot - outlet annular tube

I - ZONE I

II - ZONE II

References:

1. Tayo Kaken Company, A means of reactivating worked charcoal, *Japanese patent* 50-48301 (1975)
2. Petkovska, M.; Tondeur, D.; Grevillot, G.; Granger, J.; Mitrović, M., Temperature-swing gas separation with electrothermal desorption step, *Sep. Sci. Technol*., **26**, 425-444 (1991)
3. Sullivan P., "Organic vapor recovery using activated carbon fiber cloth and electrothermal desorption", *Ph.D. Thesis*, University of Illinois at Urbana-Champaign, 2003
4. Petkovska M. and Mitrovic M., "Dynamics of electrothermal desorption process: heterogeneous, one-dimensional macroscopic model", *J. Serb. Chem. Soc.*, **57**, (1992), 319
5. Willadsen J. and Michelsen M.L., "Solution of Differential Equation Models by Polynomial Approximation", Prentice-Hall, Inc. Inglewood Cliffs, New Jersey, 1978
6. Perry's Chemical Engineer's Handbook*, The McGrawHill, 7th* edition, (1999)
7. Fuentes, J., Pironti, F., Lopez de Ramos, A. L., Effective Thermal Conductivity in a Radial-Flow Packed-Bed Reactor, *International Journal of Thermophysics*, **19**, 781-792 (1998).
8. Stuke, B., *Angewandte Chem.*, **B20**, 262 (1948).
9. Ruthven, D.M., Principles of adsorption and adsorption processes, *J. Wiley & Sons,* New York, 1984
10. Lo, S.Y., Characterization of the chemical, physical, thermal and electrical properties of a series of activated carbon fiber cloths, *Sc. M. Thesis*, University of Illinois at Urbana-Champaign, 2002
11. Bathen, D., "Adsorption Processes in Environmental Technology", *3rd European Congress of Chemical Engineering ECCE-3*, June 2001, Nuremberg, Proceedings on a CD
12. Subrenat A. and Le Cloirec P, "Industrial application of adsorption onto activated carbon cloths and electro-thermal regenearation", *Journal of Environmental Engineering*, 2004 (in press)
13. Incropera F.P. and DeWitt D.P. Fundamentals of heat and mass transfer, *J. Wiley & Sons*, New York, 1996